Liquid Phase Sintering of a novel Tungsten Heavy Alloy with High Entropy Alloy as Binder

By

Zahid Anwer

School of Chemical and Materials Engineering

National University of Sciences and Technology

2019

Liquid Phase Sintering of a novel Tungsten Heavy Alloy with High Entropy Alloy as Binder

Name: Zahid Anwer

Reg. No: 00000118124

This thesis is submitted as a partial fulfillment of the requirements for the degree of

MS in Materials and Surface Engineering

Supervisor Name: Dr. Malik Adeel Umer

School of Chemical and Materials Engineering (SCME)

National University of Sciences and Technology (NUST)

H-12 Islamabad, Pakistan

August, 2019

Dedication

I would like to dedicate this work to five people who I love the most and continue to mean so much to me. Firstly, my late father Mr. Muhammad Anwar, my mother, my wife Sanober Saeed, my little daughter Irhaa Zahid and last but not the least my sister Sadia Umair.

Acknowledgments

Alhamdulillah, all praises to **Allah** Almighty for providing me the strength, courage and blessing to complete this thesis.

Special gratitude goes to my supervisor, **Dr. Adeel Umer** for his supervision and constant support. His invaluable help of constructive comments, suggestions and guidelines throughout the experimental and thesis work have contributed to the successful completion of this research work. Not forgotten, my appreciation to GEC members **Dr. Muhammad Mujahid** and **Dr. Khurram Yaqoob** for their support in terms of guidelines and knowledge regarding the research topic.

I would like to express my special appreciation to **Dr. Badar Rasheed** and **Miss. Farah** for their utmost facilitation in carrying out experimental work during my research. I would like to extend sincere thanks to all my friends: especially **Syed Bilal Tayyab Gilani** for helping me through preparation and characterization of samples; **Mr. Azam Hafeez** and **Mr. Abdul Mannan** for their continuous support and encouragement throughout my research work; and **Mr. Faisal Razzaq** for making experimental arrangements, out of tight production schedule. I would like to appreciate **Mr. Qamar-ud-Din** for his sincere assistance in carrying out SEM/EDS characterizations.

Lastly, I must express my very profound gratitude to my parents, my in laws, my spouse and sibling for providing me with unfailing support and continuous encouragement throughout my years of study and through the process of researching and writing this thesis. This accomplishment would not have been possible without their valuable support and prayers. Thank you very much.

Zahid Anwer

Abstract

High entropy alloys (HEA) are a new class of materials, in which five or more principle elements are incorporated in equal or near equal atomic (%) ratios. Unlike conventional alloys, with one principle element, these alloys offer an exciting set of properties without compromising on existing ones. Hence, HEA warrant their exploration for systems that have previously been researched and still require improvements in their properties.

Tungsten heavy alloys have been the industrial standard for applications, requiring high density, vibration damping, counter balancing, kinetic energy penetrators etc. However, for kinetic energy penetrators depleted uranium are still the best contender than tungsten heavy alloys. Currently, tungsten heavy alloys are being manufactured as composites; wherein, tungsten particles are embedded inside ductile matrix of a fcc Ni-Fe alloy system, in which Co and Mn are added to improve mechanical properties of the composite.

Keeping in view the presence of four elements in the binder matrix of conventional tungsten heavy alloy, this research work aimed at studying the possibility of manufacturing a high entropy alloy-based matrix by adding Cr into the basic four elemental system by keeping the inclusion of each element between 14% - 22% atomic.

The powders after mixing were subjected to undergo liquid phase sintering under two different environments i.e. pressure-less sintering and hot iso-static pressing (HIP) sintering, respectively. Microstructure was analyzed by SEM/EDS, crystal structure and phase analysis were conducted through XRD analyses. The mechanical tests in regimes of hardness, impact and compression were conducted and the results were compared with the conventional tungsten heavy alloys. Liquid phase sintering under HIP sintering was found to be successful in obtaining the classic liquid phase sintered structure, in which tungsten particles are embedded inside binder matrix.

Table of Contents

List of Figures

List of Tables

Abbreviations

1. P/M;	Powder Metallurgy
2. WHA;	Tungsten Heavy Alloys
3. DU;	Depleted Uranium
4. APFSDS;	Armor Piercing Fin Stabilized Discarding Sabot)
5. NUST;	National University of Science and Technology
6. RHA;	Rolled Homogenous Armor
7. HEA;	High Entropy Alloys
8. FCC;	Face Centered Cubic
9. BCC;	Body Centered Cubic
10. VEC;	Valence Electron Concentration
11. BSE-SEM;	Back Scattered Electron – Scanning Electron Microscope
12. XRD;	X-ray Diffraction
13. EDS;	Energy Dispersive X-ray Spectroscopy
14. HEA-WHA;	High Entropy Alloy based Tungsten Heavy Alloy
15. HIP sintering;	Hot iso-static pressing sintering
16. W-HEA;	High entropy alloy-based tungsten heavy alloy
17. W-Ni-Fe;	Conventional tungsten heavy alloy (industrial standard)

Chapter 1

1.1 Tungsten Heavy Alloys

The meaning of "Tungsten" in Swedish language is "Heavy Stone", it comes under the class of refractory metals with the highest melting point of 3420˚C [1]. Tungsten is the material of choice when it comes to the high temperature applications [2]. As the name suggests, tungsten is really heavy with a density of 19.3 g/cm^3 and also very hard but for certain applications tungsten is too hard and brittle therefore, in order to cater this shortcoming; composites of tungsten are manufactured along with tougher matrices [3]. One such approach is applied for the development of kinetic energy penetrators for armor piercing application, in which Tungsten Heavy Alloys (WHA) are utilized to provide the necessary impact and perforation.

WHA (with elemental composition of W-Ni-Cu) were first developed in 1930's, laying the theoretical grounds for liquid phase sintering [4]. In these alloys tungsten is maintained between 80-98% while rest of the elements form the matrix, given in figure 1 is the conventional microstructure of a WHA, in which Tungsten particles are embedded inside a Nickel and Copper matrix [3].Thus, a bi-constituent system is formed called composite, which provides a good combination of hardness, strength and toughness. Two systems of WHA comprising of W-Ni-Fe and W-Ni-Cu have been explored in which Ni, Fe and Cu serve as binder (matrix) to integrate the hard tungsten particles together to impart toughness and machinability. WHA are material of choice for all such applications which demand high specific weight of materials for example; counter weights for balancing, hazardous radiations shields, machining tools and munitions etc. [3][5].

1.1.1 Kinetic Energy Penetrators

During World War II, tungsten carbide based penetrators were used but because of their inferior toughness property they tend to break upon impact thus, a need for the development of new alloys was felt and efforts led to the development of WHA hence, the same were explored during 1960-1973 [1]. It was 1973, when Depleted Uranium Alloy was trialed for penetration purpose and till date it is the best available choice in terms of perforation capacity however, because of Uranium's toxic nature its usage

has been discouraged and therefore, research is being carried out to upgrade the performance of WHA, which are non-toxic and environmental friendly [1].

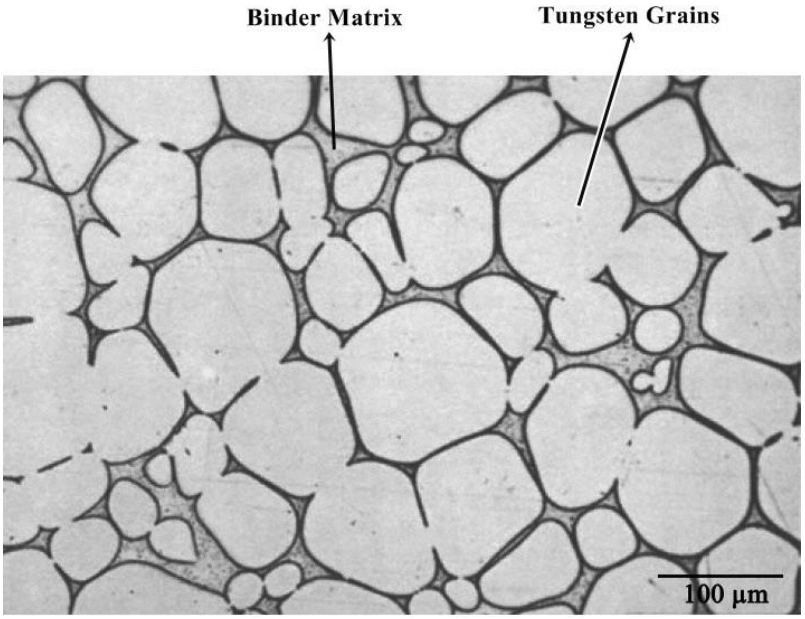

Figure 1. Microstructure of a liquid phase sintered Tungsten Heavy Alloys

Kinetic energy penetrators belong to the class of anti-tank ammunitions, which are designed to perforate through the armor by making use of its kinetic energy. In this class of munitions, the APFSDS is considered to be the most destructive one [1]. Kinetic energy is directly depended upon the density of penetrator and therefore, it is desirable to manufacture penetrators from such materials which are hard, dense and tough[6]. A comparative study of mechanical properties and fracture mechanism revealed that penetrators made from W-Ni-Fe were better than W-Ni-Cu as the former exhibit better density however, shows poor interfacial strength between matrix and tungsten particles and lower tensile strength as compared to the later one [7].

1.1.2 The Mushrooming Effect

Owning to the high melting point of Tungsten, the effect of thermal softening in WHA is less pronounced and associated with less thermal softening is a delayed initiation of adiabatic shear bands which primarily controls the consumption rate and sharpness of the penetrator. This delay makes the strain hardening overcome thermal softening thereby, leaving the penetrator to deform into a mushroom like heads during the perforation through armor [1], [2], [8].

1.1.3 Adiabatic Shearing

It is a phenomenon witnessed at higher rate of deformations, contrary to the ideal materials this shearing mechanism is manifested by real materials and thus, is called to be the inherent material property [9]. Metals undergo plastic deformation by the interaction and motion of dislocations or line defects [10][11]. When metals are cold worked i.e. application of force / stresses at normal room temperature, they undergo plastic deformation and some part of this work is stored as elastic strain energy while rest of the work is dissipated in the form of heat energy. Experimental evaluation of cold working has revealed that, the dissipation of total work into heat energy accounts for almost 90 to 95% [9]. Practically, during the dynamic deformation a definite fraction of the heat energy is lost to the environment which depends upon the rate of deformation and thermal properties of metals. However, in situations where time between plastic deformation and dissipation of heat is in fractions of seconds then, this heat energy is retained inside the metal system due to which the whole deformation mechanism alters and this alteration is known as adiabatic shearing [9].

The penetrator strikes the armor at a very high velocity of approximately 1-2 Km/s [1] therefore, the deformation rate of penetrator is extremely high. Due to such a higher deformation rate the time required for the heat energy to dissipate, generated because of plastic deformation, is immensely short thus, leaving the system into an adiabatic system[1]. When metals undergo such large plastic deformations, a phenomenon called localization of plastic flow tends to occur because of the heating in the localized regions. This kind of localized flow is often accompanied by a sudden or catastrophic fracture by immense localized shearing specifically called the adiabatic shearing. Therefore, adiabatic shearing is mainly caused because of the thermal softening which outstrips the effects of strain hardening; this is the point where metals become thermally instable [8]. Therefore, the catastrophic failure occurs by adiabatic shear bands which are the ultimate means of penetrator consumption. *The rate of penetrator consumption can be co-related with the initiation of shear bands i.e. faster the initiation of adiabatic shear bands, fewer will be the consumption rate of penetrator*

[1] Adiabatic System, is a system in which no heat enters or leaves the system that is heat energy remains inside the system [59]

in terms of per unit of length [8]**.** The same is seen in the Depleted Uranium penetrator and this is the reason why they are more efficient than WHA penetrators.

1.2 Powder Metallurgy

P/M is a processing route which is known to the mankind since 3000 B.C [12], when Egyptians made use of this technique for manufacturing of tools by reducing the iron ore [13][5]. By the time, this manufacturing approach evolved and in 1826 Russians raised P/M to the commercial utilization level by sintering a compressed powder at high temperature. The ability to manufacture finished components in a single cycle, marked a new era for P/M in which fabrication of Copper-Silver-Lead based coins and cementing of platinum were among the prominent applications. The inception of new era for P/M began with the development of Tungsten filament by Coolidge for Thomas Edison. Thereafter, manufacturing of Tungsten Carbides, Copper-Tin bearings and Cupro-Graphite connectors were emerged in the decade of 1930. Consequent to the continual research in the field of P/M, various Tungsten, Iron and refractory alloys were developed by 1940 [14][3].

The crux of P/M can be described as, a mixture of powders is chosen depending upon the desired properties for an application then this mixture is die-pressed under a pressure range of 98-980 MPa. This compact is now called a green compact, which is delicate nevertheless suitable for handling to the next processing step. This green compact is then exposed to higher temperature treatment known as sintering. Sintering is conducted, in a temperature range, below melting point of the major constituent i.e. almost 66-75% of melting point[15]. A general layout of P/M is presented in Figure 2 [5].

P/M has provided new avenues of industrial manufacturing where tailor made commercial products can be produced without melting, casting and machining processes. This technique has not only provided an alternative manufacturing route, but also made the utilization of refractory materials quite easier and practical. P/M has solved the problem of insolubility of metals, with higher melting point differences, for example Tungsten (3410˚C) and Copper (1085˚C) [16] moreover, manufacturing of a single system (composites) based up on the heterogenous components like metallic and non-metallic; can also be produced via P/M. It is owning to the diversities associated with P/M, which brought revolution in the fields of cutting, mining,

aerospace, automotive, military, electronics, electrical and telecommunication industries to mention the least [15].

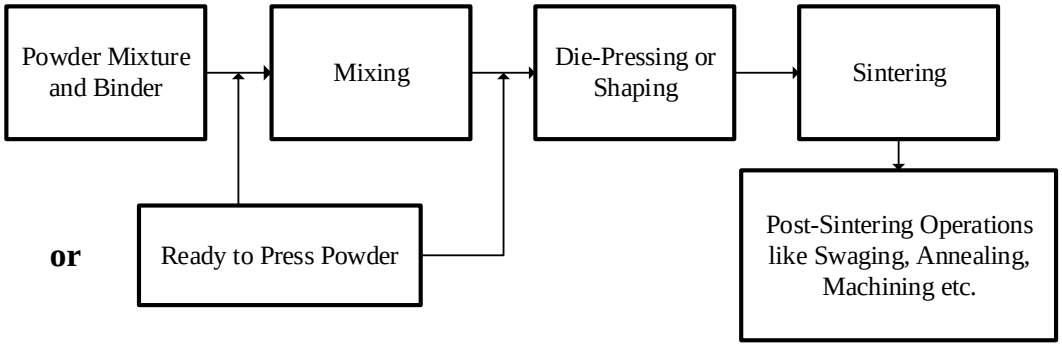

Figure 2. General layout of parts manufactured by P/M.

1.2.1 Sintering

It is a thermal process which facilitates the bonding of particles together which in turn, provides strength and mechanical stability to its green compact. As mentioned in the preceding section, this process is carryout at temperature which below the melting point of major constituent. The driving mechanism of sintering is solid-state diffusion of atoms [5], [14]. Sintering is a processing step in P/M, which is one of most basic and influential elements that govern the final properties in the field of Materials Science & Engineering [5], [16], [17]. Sintering therefore, defines the microstructure which in turn defines materials properties. Thus, the grains size, grain structure, sinter density and distribution of phases along with pores are the key parameters to consider. Intrinsically, sintering can be divided into: Solid-State Sintering and Liquid-State Sintering.

1.2.1.1 Solid-State Sintering

In solid-state sintering, the complete densification of powders occurs in the solid phase at materials-specific temperature also known as the sintering temperature [5]. The driving force behind this type of sintering is reduction in the surface-volume ratio, which is very high in powders.

1.2.1.2 Liquid-State Sintering

In liquid-state sintering, a liquid state co-occurs with solid powders at the sintering temperature and liquid tends to fill pores and impart discontinuity between solid powders i.e. decreasing contiguity. Normally this liquid phase acts a binder or matrix

which holds the brittle or hard particles together thereby, providing ductility and toughness to the final composite / bi-constituent phase system [18].

Generally, liquid-state sintering permits a rather easier control over microstructure and properties than solid-state sintering moreover, it is economically more viable and therefore is frequently used at industrial level [5]. Solid-state sintering is still a better choice and mostly utilized for manufacturing of ceramics.

1.2.1.2.1 Stages of Liquid Phase Sintering

Liquid phase sintering has some notable effects on the microstructure of the sintered object. The liquid performs two basis tasks:

1. It wets the solid particles
2. It dissolves the solid to reduce particle to particle contact or contiguity

By doing so, the liquid fills up the gaps and the overall interfacial energy of the system is reduced. In tungsten heavy alloys, the liquid tends to remain present throughout the isothermal holding temperature which is also known as the sintering temperature. This presence of liquid accounts for providing a fast densification along with grain growth.

In a given classic system the liquid phase sintering occurs in three stages:

1. Liquid Formation; it is accompanied by rapid densification since, the liquid starts to spread by virtue of capillary forces however, it is essential for the liquid to offer a sufficient wettability for solid particles.
2. Solution-reprecipitation, coarsening of microstructure or Ostwald ripening takes place when the small in size grains dissolve in nearby liquid and eventually become part of larger grains.
3. Solid State Sintering or grain growth, during this last stage increases the contiguity and therefore, it is desirable to shorten its duration to a lowest possible period of time.

1.2.1.3 Densification

Densification of products plays a vital role for achieving the high-performance standards. Thus, it is imperative to monitor the residual porosity in the microstructure and devise methods to minimize them and attain maximum possible densification. Thus, one can deduce that attainment of full density and getting rid of pores is a challenge in P/M [14]. With extending the sintering time the structure of pores

becomes more stable especially when gas is filled inside them, at this stage it is near to impossible to diffuse out pores from the compact [5]. Thus, a fast diffusing gas e.g. Hydrogen gas is utilized to get rid of all entrapments. Another approach to attain sound densification and that too in a shorter period of time is by liquid phase sintering, as in liquid state the diffusion of atoms is faster than in solid-state and by virtue of capillary force it fills up gaps and excavate entrapped gas out of the compact in a robust manner [18].

1.2.1.4 Grain Growth

Grain growth is directly associated with temperature and holding time i.e. the average grain size of a compact increases as the holding time at a given temperature increases. With the changing grain size final properties of the product also changes [19] the finer grains offer higher stiffness, strength and hardness with lower ductility and toughness whereas, coarser grains provide a vice versa of the same.

1.3 High Entropy Alloys

1.3.1 Introduction

The previous practices of alloy designing used to revolve around one major / base metal and further additions were made to acquire the desired properties[20]. The research work in the field of materials science and engineering encouraged the scientists and engineers to explore new frontiers and develop new and improved materials. Hence, going beyond the conventional approach, a new concept has been discovered since 1995. The term HEA was coined in 2004 by Yeh et al. who also defined this new class of alloy as, an alloy comprising of no less than five elements with each one contributing between 5 to 35 atomic percent is called a HEA. Contrary to the past experiences, as for as the synthesis, processing and analysis are concerned, up till now it has been demonstrated and validated that, these alloys are viable and completely practical [21]. However, there still exists an enough room that needs to be explored to optimize and materialize this class of alloys to its maximum possible potential.

The beauty of this alloys lies in the multi-principal elemental composition which tends to render them a special set of properties in higher regime like strength, hardness, high temperature stability, wear resistance, structural stability and corrosion resistance [22].

Usually in conventional alloys, a compromise among the properties has been observed i.e. ductility is attained at the expense of reducing strength and vice versa. On the other hand, HEA are such a promising class of alloys which can provide an amazing set of properties without a significant compromise between the rest ones [22]. Moreover, these alloys can be made in conventional ways by using the conventional processing routes thus, can be utilized in industries for mass production of products as well. Today a lot of advanced application require new materials which includes Engines, Nuclear, Marine, Defense etc. Some currently in use examples of HEA are $Al_5Cr_{12}Fe_{35}Mn_{28}Ni_{20}$ (good workability), $Co_{1.5}CrFeNi_{1.5}Ti_{0.5}$ (high temperature strength and oxidation resistance) and $Al_{0.3}CrFe_{1.5}MnNi_{0.5}$ (good wear resistance by profile hardening) [23].

Pioneer work in the field of HEA was carried out by Cantor along with Alain Vincent, who was Cantor's student back in 1981[23]. Their work started by developing numerous multi-component / equiatomic alloys and they experimented with up to 20 elements which is also a world record for multi-component alloy. Out of these experiments they found out just one alloy which gave a single solid solution i.e. FCC and it was $Fe_{20}Cr_{20}Ni_{20}Co_{20}Mn_{20}$ the result were published in 2004 by Canter et al. he synthesized this alloy by melt spinning [20]. Further details regarding the research progress which incubated upon this very work of Cantor is discussed in chapter two.

Brian Cantor in 2014 has shown the possibility of total number of alloys that can be manufactured and trialed and a practical estimate by using Gibbs phase rule as an underlying principal came out to be 1078 [24] which is an extremely high number. The solubility of various components into one another can be adjudicated by making use of the famous Home-Rothery Rules including parameters like crystal structure, atomic size difference, valency and electronegativity difference. Yeh et al defined HEA and also highlighted the fact that the configurational entropy of these alloys is always high owing to the fact that greater the number of components in an alloy, greater will be its configurational entropy or mixing entropy. He also emphasized upon the fact that configurational entropy has an influential effect upon the microstructure and properties of HEA. Unlike conventional alloy systems, high mixing enthalpy is coupled with an enhanced solubility of various equiatomic or near-equiatomic components; leading to simple microstructures with minimum complexities [25]. It is owning to this very concept which has become the motivation for researchers to explore new materials

with novel properties and therefore extensive study is being carried out on this new class of alloys.

1.3.2 Alloy Designing of HEA

As mentioned in the aforementioned section, there exists a huge possible combination i.e.10^{78} hence, basic rules of materials science are followed while selecting the type of elements moreover, making the most modern technology the likes of computational thermodynamics is also being used in the form of CALPHAD; which predicts a reasonable phase diagram for HEA and also by using the parametric approaches like valence electron concentration [23][26].

1.3.2.1 Valence Electron Concentration

VEC is a parametric approach based upon physiochemical properties of the alloying elements which is reasonably useful for predicting the formation of solid solution in HEA [26]. VEC makes use of the available data of elements for prediction like atomic radii of elements, mixing enthalpies and melting points [27][28][29].

VEC has been renowned of not just controlling the stability of phases but also the properties of alloys [28]. VEC is basically defined as the total number of electrons present in the valence electron band of an element including the d-orbitals such as, VEC value for copper is 11 etc. Previously, VEC method had been used to effectively control the ordering of a crystal structure in Co_3V and Fe-Ni system. Therefore, the elements iron, nickel and cobalt have similar atomic radii and electronegativities hence, VEC values can be utilized for prediction of the HEA solid solutions [30]. Guo et al. has experimentally tested the applicability of VEC rule [31] and hence, following are the conclusions drawn on qualitative and almost quantitative basis in Table 1-1 [32]. The validity of VEC rule have been carried out by synthesizing through casting however it has yet to be explored for sintering / powder metallurgy and there are several conditions that apply for 100 % applicability of this rule, for detailed study readers are referred to the cited reference [26]. However, keeping in view the vast possible combinations of multi-component alloy one can consider in soliciting help through this rule and some new experiments may also validate its use in future.

VEC has previously been defined according to the following equation[33]. According to this equation the cumulative value of VEC can be calculated by adding up all the

value that comes after multiplying individual values of VEC for each respective element with its relative concentration "c". The cumulative values can then be related with the values given in table 1 for crystal structure prediction.

$$VEC = \sum_{i=1}^{n} C_i(VEC)_i \quad \text{.....[1]}$$

Table 1-1. Generalized solid solution predication by VEC

Qualitative Basis	
Higher Values of VEC	FCC
Lower Values of VEC	BCC
Intermediate values of VEC	FCC + BCC
Quantitative Basis	
VEC $\geq$ 8	FCC
VEC < 6.87	BCC
6.87 $\leq$ VEC < 8	FCC + BCC

1.3.3 Thermodynamics of HEA

To understand the concept behind high entropy alloys one must refer to the principles of thermodynamics, which states that ; under the isothermal ($\Delta T = 0$) and isobaric ($\Delta P = 0$) conditions, a system will always prefer to attain equilibrium by lowering its Gibbs free energy (G)[34] equation (1), provides the relation among Gibbs free energy, enthalpy (H), Temperature (T) and entropy (S):

$$G = H - T\Delta S \quad \text{..... [2]}$$

The equation reveals that at any given temperature, in order to attain equilibrium enthalpy and entropy are directly proportional to the Gibbs free energy and the most stable state will be the one with lower enthalpy and higher entropy hence, a best compromise between H and S will give the lowest value of G[35]. Therefore, in order to predict the equilibrium state of an alloy, the total free energy change from elemental to combined form is compared so as to ascertain which state or phase has the lowest mixing Gibbs free energy (ΔG_{mix}) hence, equation 1 can be rewritten as[34]:

$$\Delta G_{mix} = \Delta H_{mix} - T\Delta S_{mix} \ldots\ldots\ldots\ldots\ldots\ldots [3]$$

The mixing entropy in equation (2) can be calculated through Boltzmann's hypothetical equation i.e.

$$\Delta S_{mix} = R\ln(n) \ldots\ldots\ldots\ldots\ldots\ldots [4]$$

In equation (3) R is general gas constant with value 8.314 J/K.mol and *n* is the number of components or elements in an alloy present in equimolar or near equimolar quantities. It can be seen in equation (3) that, my increasing '*n'* the value of ΔS_{mix} also increases. That is the basic reason behind stability of solid solutions at lower temperatures when the inter heat i.e. enthalpy of the system is lower and with increasing '*n*' mixing entropy of the system increases which in turn lowers the overall Gibbs free energy of the system thus, rendering it stable and viable. It is owing to their high mixing entropy which rendered multielement alloys (having a minimum of 5 elements and 5-35 atomic%) the name of "High Entropy Alloys".

The Boltzmann's equation explains why do HEA form single or mixed solid solutions. With greater values of 'n' comes greater possible configurations; binary alloys with just two components have limited possible configuration and that is why they form terminal solutions and compounds instead of complete solid solutions phases [34].

Chapter 2

2.1 Literature Review

The driving force behind carrying out research on WHA, for penetrators, is the hazardous environmental concerns of DU alloys. In comparison to DU alloys, WHA tend to exhibit an inferior perforation equaling to about 10% [6]. Therefore, efforts are in progress to mitigate for this 10% performance difference and elimination of the associated deleterious effects of DU alloys.

2.2 Processing of WHA

As mentioned in 1.1 WHA were first produced in 1930s, the conventional way to produce these alloys is via P/M. The alloys are normally liquid phase sintered however, mechanical alloying and infiltration is also being used depending upon the application and properties requirement. Liquid phase sintering is commonly used for WHA as this process offers sintering at lower temperature, better densification, uniform microstructure and sintered densities that are quite near to the theoretical densities. Moreover, for a mass production point of view this processes is quite favorable as well, hence associated with liquid phase sintering are some considerable benefits [36].During the processing of WHA one of the key factors is to cater for the oxidation and purity levels of powder being used. The oxides tend to lessen the densification of final alloy by majorly increasing the porosity levels inside the sintered compact and as discussed in **1.2.1.3** associated with density are the final properties of alloy therefore, the utilization of a reducing environment for example Hydrogen, Nitrogen, a mixture of thereof may be incorporated to out gas the inherited oxide inside the powder mixture. The technical / normal practice to reduce the oxides inside (W-Ni-Fe WHA) the powders is by applying isothermal holds at 900˚C and 1150˚C for about 1 -1/2 hours in a hydrogen environment. Secondly, in order to avoid the blistering, precipitation and impurity segregation, it is imperative to use the maximum possible pure grades of powder because they too alter the final properties of WHA [3][6][37]. Isothermal holds may accompany with hydrogen embrittlement this problem can be sorted out by changing the environment from hydrogen to an inert gas for example argon [38][39]. As an alternative solution a process known as glowing is carried out which is a post-sintering operation in which WHA are annealed in a vacuum

environment to expel the remaining hydrogen gas inside the compact and also to suppress the deleterious effects of hydrogen embrittlement [6]. Prolonged exposure of WHA in hydrogen environment results in coarsening of pores which makes the alloy brittle thus, reduces the ductility which is one of the key parameters in high deformation rate applications like kinetic energy penetrators [38]. Shrinkage porosity, more pronounced in W-Ni-Cu alloys, is another problem which occurs during liquid phase sintering, in this kind of defect severe internal cracks do form, this problem can be tackled by slowly cooling down the compact from isothermal sintering temperature to solidus temperature of the matrix [37].

2.2.1 Microstructure and Mechanical Properties of WHA

During the early development in WHA, the main focus was to improve the static or pseudo-static mechanical properties hence, it was believed that final properties are entirely depended upon the tungsten content while, binder's influence is negligible [6]. In 1.1.3 it has been explained, why the need for initiation of adiabatic shearing is instrumental in boosting the perforation capability of the kinetic penetrator. Ramesh and Coates tested W-Ni-Fe WHA on high strain rate and found out that post sintering operation like swaging makes the WHA less rate sensitive [40]. Hence, by reducing the rate sensitivity and promoting an earlier formation of adiabatic shear bands, penetrator's performance could be enhanced. Moreover, it is also desirable that the direction of crack propagation should preferentially be along the shear band. To make this possible WHA must have a lower W-W contiguity, as greater tungsten to tungsten interface makes the formation of shear bands rather difficult to form. This can be achieved by either reducing the tungsten content inside WHA and increasing the binder content, but this would reduce the overall density of penetrator which in turn would lessen the kinetic impact. Thus, a balance must be acquired which not only avoids the compromises on density but also facilitates the adiabatic shear band formation thereby, eliminating the 'mushrooming effect'. Another approach to reduce the W-W interface is by increasing the grain size of tungsten but R.M. German and L.L. Bourguignon [6] found out that the elongation and ultimate tensile strength both decrease by increasing the grain size of tungsten. This was attributed to the fact that larger grain size will initiate a larger crack at the W-W grain boundary and thus will render the WHA as weak [40]. The relationship between W-W contiguity and an increase in the tensile strength & elongation was also showed by R.M. German and B. Rabin [41]. A new

approach of reducing the tungsten to tungsten contiguity is by cyclic heat treatment after sintering [42]. This cyclic heat treatment would involve an overlapped isothermal hold and quench events just after the binder has reached to its solidus temperature. Due to the cyclic heating & cooling cycle and the difference in the co-efficient of thermal expansion for tungsten and binder, the matrix tends to infiltrate the W-W grains thereby, reducing the W-W contiguity [1]. Similar, results were reported by Upadhyaya when a reduction in contiguity up to 50% was achieved in tungsten carbide and cobalt system; which resulted in an increase in toughness without comprising the wear / abrasion resistance [6]. One of the efforts made for early start up adiabatic shearing in WHA was in the field of surface engineering in which the surface of the penetrator was case carburized and better results were reported at 800 ˚C for 2 hours [43].

2.3 Novel Tungsten Alloys / Composites

2.3.1 Tungsten with Intermetallic Bonds

In order to promote the adiabatic shearing in WHA, the binder was modified with an intermetallic compound Ni_3Al [44]. This intermetallic compound showed a temperature dependent strengthening mechanism for tungsten alloy in such a manner that a rise in the yield strength took place up to 700 ˚C and above this temperature nickel aluminide losses its strength. This anomalous behavior of nickel aluminide showed an early onset of adiabatic shear bands, moreover crack propagated along the adiabatic shear band.

2.3.2 Tungsten-Silica Composites

To facilitate the self-sharpening in WHA instead of mushrooming, SiO_2 was added in tungsten. The idea was to utilize the brittleness of these particles for localized shearing of alloy [6]. The major benefit of utilizing silica in tungsten was that it tends to set into the grains of tungsten rather than on grain boundaries. Thus, it was expected to initiate the adiabatic shearing in tungsten without comprising the tensile strength. This process was carried out via solid state sintering however, to ensure through mixing mechanical alloying was carried before sintering. Results showed an improved perforation with an early start to the adiabatic shearing.

2.4 FeCrNiCoMn Alloys

Among the numerous high entropy alloys discovered till date, the FeCrNiCoMn system is the single one, with FCC crystal structure, that has been studied or explored quite extensively. This system usually competes with BCC, σ-phase and HCP crystal structures. The σ-phase normally comes from cobalt and chromium as can be seen in figure 3 (a). However, with the addition of more components the σ-phase can be limited or eliminated see figure 3[26].

As mentioned in 1.3.3 the phases compete within a system and the one with lowest Gibbs free energy emerges as the equilibrium phase. Similarly, in the case of FeCrNiCoMn system σ-phase, BCC is coexisting equilibrium phases with FCC and therefore in figure (4) these phases are studied with respect to the thermodynamic properties namely Gibbs free energy, enthalpy and entropy. During this examination

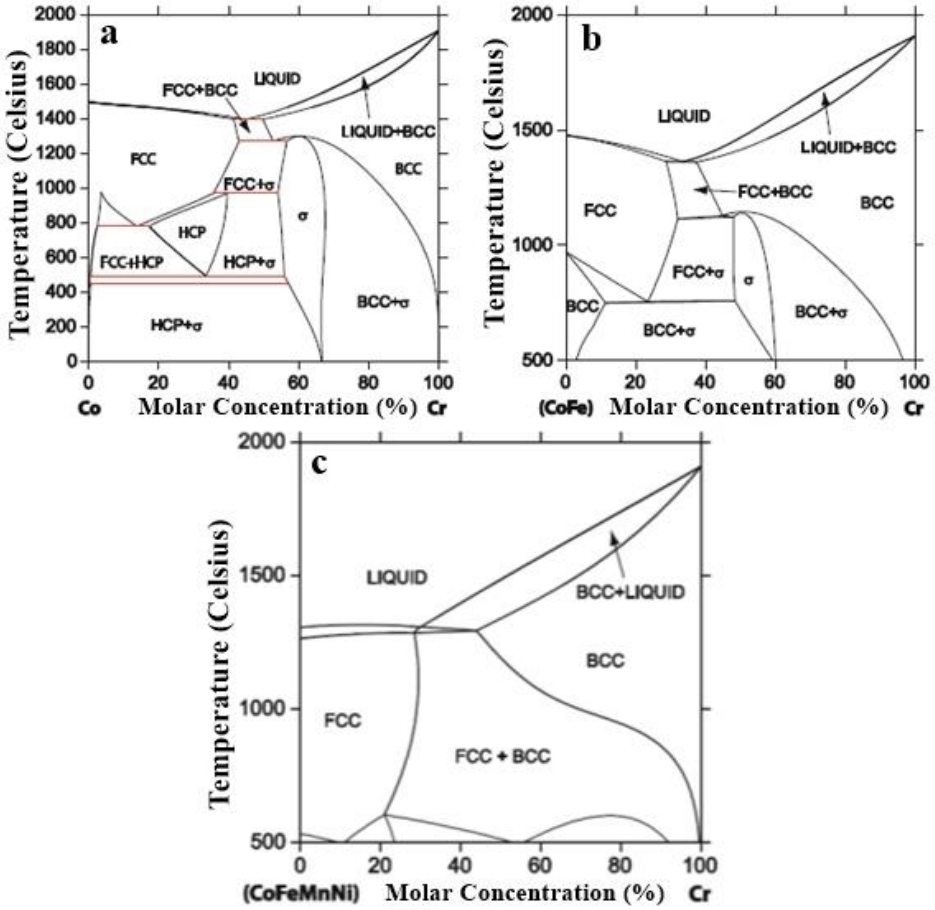

Figure 3. (a) Binary phase diagram of Cobalt and Chromium (b) CALPHAD – pseudo binary phase diagrams Cobalt, Iron and Chromium it can be seen with adding one more element i.e. iron, the σ-phase is shrinking (c) Cobalt, Iron, Manganese, Nickel and Chromium with the addition of 3 more elements i.e. iron, manganese and nickel the σ-phase has been eliminated leaving behind FCC and BCC solid solution phases.

the concentration of chromium has been varied however, the calculations have been carried out at a temperature of 1000˚C[26]. It can be observed that with the addition of chromium the FCC and BCC structures are becoming more favorable than σ and HCP phases. This stabilization can be attributed by the contribution of enthalpy and entropy. With the addition of chromium into CoFeMnNi the enthalpy for FCC and HCP is decreasing, entropy for BCC and FCC is highest but FCC has lower value for Gibbs free energy up to 40 at%. The results show that both enthalpy and entropy must be considered along with Gibbs free energy for predicting of equilibrium phases. Figure (5) shows the mixing properties of FCC phase at 1000˚C for different systems like:

1. Co-Cr binary,
2. Co-Cr_x-Fe tertiary,
3. Co-Cr_x-Fe-Ni quaternary,
4. Co-Cr_x-Fe-Ni-Mn quinary.

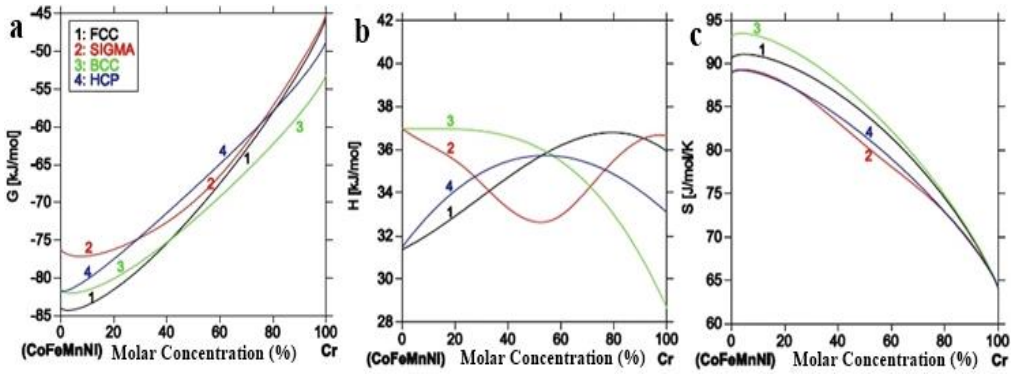

Figure 4. CALPHAD – TCNI7 database at 1000˚C with varying chromium molar concentration (a)lower Gibbs free energy for FCC and BCC (b) lower Enthalpy for FCC and HCP (c) Higher Entropy for BCC and FCC.

2.4.1 Gibbs free energy of mixing

The figure 5 (a) shows in a given system, with the increase in number of components the value of ΔG_{mix} decreases for all the systems monotonically; over the entire mole % Cr range. And referring to 1.3.3 this is because of lowering of enthalpy of mixing and rising of mixing entropy.

2.4.2 Enthalpy of mixing

In figure 5 (b) the enthalpy of mixing decreases and eventually becomes negative for the quinary system having chromium mole % up to 40%.

2.4.3 Entropy of mixing

The dotted lines in Figure 5 (c) shows the ideal mixing and all the systems have shown the increase in their mixing entropies. The ΔE_{mix} of Co-Cr have even exceed the ideal configurational entropy of mixing line for a tertiary alloy system.

2.5 Statement of the problem

The delay in the initiation of adiabatic shear bands in WHA results in the mushrooming effect or bending of penetrator tip which in turn neutralizes the perforation ability and thus, renders it ineffective as compared to the Depleted Uranium. Uranium is environmentally hazardous moreover, its after affects are long-lasting and therefore, efforts are required to cater for this reduced performance in WHA. High entropy alloys have been reported to offer a balanced and outstanding set of properties than conventional alloys. It is therefore, encouraging to investigate HEA as binder for WHA.

2.6 Purpose of the study

The purpose of this research work is to explore the possibility of in-situ manufacturing of a novel tungsten heavy alloy with a high entropy alloy-based binder matrix through conventional methods of manufacturing and comparison of properties with the industrial standard tungsten heavy alloy.

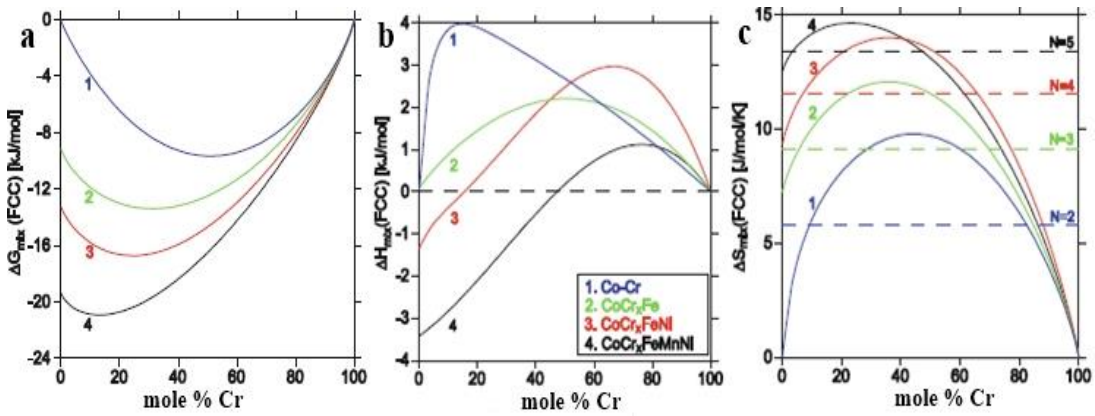

Figure 5. Thermodynamic properties of mixing for FCC at 1000˚C in various multi-component systems (a) Gibbs free energy of mixing (b) Enthalpy of mixing (c) Entropy of mixing.

Chapter 3

3.1 Proposed Solution

Sintering of HEA with Tungsten has never been studied [26][45][22] and keeping in view the foregoing trends in making WHA a better penetrator than DU alloys it seems completely logical to put efforts in probing the possibilities to produce these alloys through P/M. Previously, HEA have been manufactured by arc melting and casting, induction heating method etc. and have been reported to offer promising properties when utilized in the manufacturing of various products as mentioned in 1.3.1 however, being a growing field of alloys, they are yet to be explored in P/M regime [26]. Because of the unconventional properties, it is hypothesized that these alloys may play a part in on setting of an earlier adiabatic shearing in WHA, improve the tensile strength & elongation and subsequently, reduce the mushrooming effect. Moreover, no previous work has been reported which would assess the in-situ fabrication of HEA through sintering of raw powder mixture.

3.2 Methodology

3.2.1 Hypothesis

Tungsten Heavy Alloys (WHA) require a binder matrix to bind the hard tungsten particles and provide necessary toughness at the time of impact. High Entropy Alloys is a new class of materials which offers promising mechanical properties and require a minimum of 5 elements in a range of 5-35 at %. WHA with High Entropy Alloy matrix can be industrially manufactured through conventional powder metallurgy route and can improve the perforation capacity of existing penetrators.

3.2.2 Industrial standard (conventional) Tungsten Heavy Alloys

Tungsten Heavy Alloys manufactured via powder metallurgy route, have been obtained from Wah Industries Private Limited (WIL, Wah Cantt.) source and their elemental compositions are mentioned in Table 3-1. It is W-Ni-Fe system in which alloying addition of Co and Mn are done to achieve the desirable final mechanical properties.

Table 3-1. Elemental Composition for Conventional W-Ni-Fe.

93W-7NiFeCoMn		
Sr. No.	**Elements**	**Weight %**
1.	Tungsten (**W**)	93
2.	Nickel (**Ni**)	4.20
3.	Iron (**Fe**)	2.45
4.	Cobalt (**Co**)	0.30
5.	Manganese (**Mn**)	0.05

3.2.3 Experimentation

High entropy alloys contain 5 principle elements therefore, procurement of 99.99% pure chromium powder was procured from Asuk Trade Limited vide invoice no. INV/17-18/107-Pb, London UK. While the remaining powders were taken from production units of WIL. In line with the ongoing manufacturing practices, two different environments were chosen for sintering i.e. pressure less sintering and hot iso-static pressing sintering (HIP).

3.2.3.1 Quantification of Powders

This section reveals the quantities of powders used for making samples see Table 3-2-2. Weight is a quantifiable entity and from this, one can calculate the number of atoms and moles. In industrial manufacturing, weight fractions are usually used and therefore the same has been used in this research project. It can be seen in that the requirement for making High Entropy Alloys is satisfied which is atomic % of all 5 or greater elements must be between 5-35 atomic %[21].

Table 3-2-2. Weight and Atomic percentage wise calculations.

No.	Elements	Atomic Mass (g/mol)	Weight (g)	Weight %	No. of Atoms [(m /A) x N_a]	Atomic Fraction	Atomic %
1	**Fe**	55.85	7.44	**21.25**	2.29E+23	0.214	**21.396**
2	**Cr**	52.00	5.25	**15**	1.74E+23	0.162	**16.221**
3	**Ni**	54.94	7.44	**21.25**	2.33E+23	0.217	**21.750**
4	**Co**	58.69	7.44	**21.25**	2.18E+23	0.204	**20.358**
5	**Mn**	58.93	7.44	**21.25**	2.17E+23	0.203	**20.275**
Net Value			**35**	**100**	**1.07E+24**	**1.00**	**100**
Note: It is a **500g** system of total 6 elements in which FeCrCoNiMn powders contribute to **35g** i.e. 7% of the total system, while Tungsten (W) makes for the remaining 93% i.e. **465g** hence, it is a **93%W - 7%FeCrNiCoMn** System.							

3.2.3.2 Powder mixing and pressing

All the powders with 99% purity, were sieved through a 120-grid size mesh. Then these powders were mixed under normal room temperature conditions in a powder mixing machine for 30 minutes. The Powder mixture was then subjected to cold iso-static pressing (pressure = 150 MPa; time = 01 minute) in dimensions equaling 40mm dia. and 250 mm length. The pressed sample is shown in figure (6) below;

Figure 6. Cold iso-statically pressed sample before

3.2.3.3 Sintering

The pressed powders were then pressure less sintered in a hydrogen gas environment and hot iso-static pressing furnace environment respectively. For pressure less sintering a vacuum/controlled atmosphere furnace (series 3600, model no. 242440-1600sd CVI) was chosen and sintering temperature and time was at 1450˚C and 60 min respectively. While, for hot iso-static pressing (HIP) sintering furnace the PVA TePla Type COD 533 R was chosen at 1450˚C for 30 min under high argon gas pressure of 30-45 bar. The sintering cycles are presented in Fig 6. Densities of sintered samples were measured through the Archimedes method. The post-sintered sample is shown in figure () below:

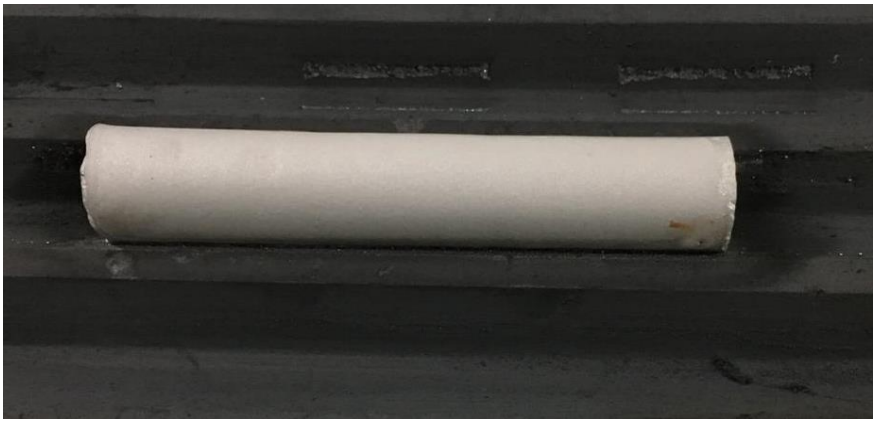

Figure 7. Post-sintered sample undergoing shrinkage due to densification during liquid phase sintering.

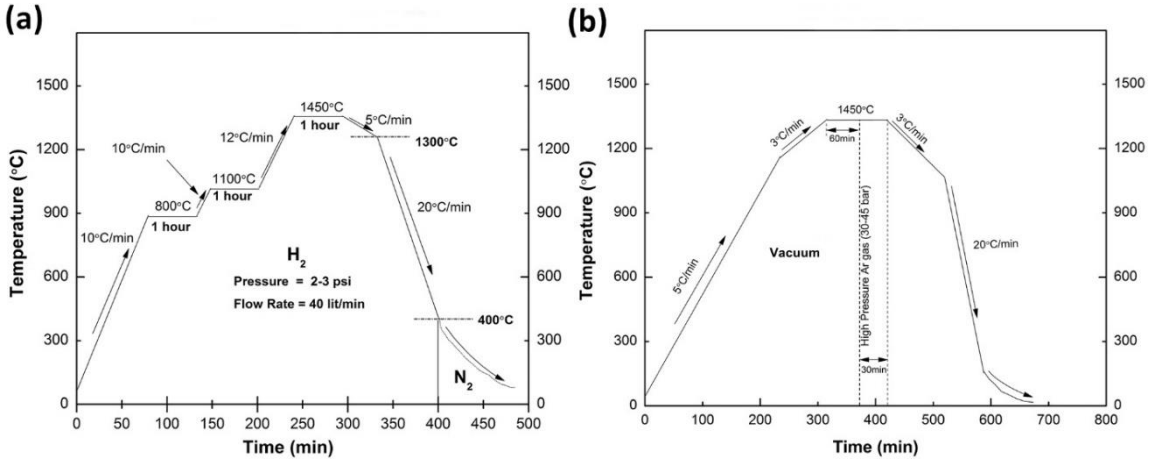

Figure 8. (a) Pressure less sintering cycle under hydrogen gas. (b) HIP Sintering cycle

3.2.4 Sample preparation and Characterization of Alloy

3.2.4.1 Microstructural Characterization

Samples were cut, grinded and polished and then microstructural characterization was carried out on Tescan Vega3 SEM.

X-ray diffraction was carried out on Bruker D8 ADVANCE with DAVINCI, a Cu Kα radiation source was used along with fluorescence and Kβ radiation filters. The diffraction patterns were obtained through a step scan mode (step size 0.020, scan rate 0.1sec) from 20˚ to 80˚(2θ).

3.2.4.2 Mechanical Characterization

Micro Vickers hardness test was conducted on FH-006 (Tinius Olsen) at 0.1 kgf and 1.0 kgf respectively. Compression Testing, as per ASTM B 925 standard (strain rate 0.005 in/in.min), of sintered samples was carried out on universal testing machine (model no. Super 602L, Tinius Olsen).

3.2.5 Results Analysis

Results were compiled, assessed and validated as per the available literature. Various softwares were used for deep analysis of results some of them are; X'pert Highscore plus for XRD analysis, Image J for contiguity and particle size distribution. Origin pro for drawing graphs, process layouts, stacking and comparison of graphs.

Chapter 4

4.1 Results and Discussion

In figure 9 is presented the SEM images of as received powders. The morphology and particle size of powders can be estimated from these SEM images. Cobalt has a solid irregular shape, chromium powder has flat or flake shape, iron has nearly spherical shape, nickel has porous/spongy shape, manganese has sharp edged particles and tungsten has a polygonal shape. Chromium, Cobalt, Nickel and Tungsten have particle sizes in the range of 2.5-3μm while, Iron and Manganese have particle sizes in the range of 5-10 μm. In figure 10 is presented the XRD patterns for the corresponding powders.

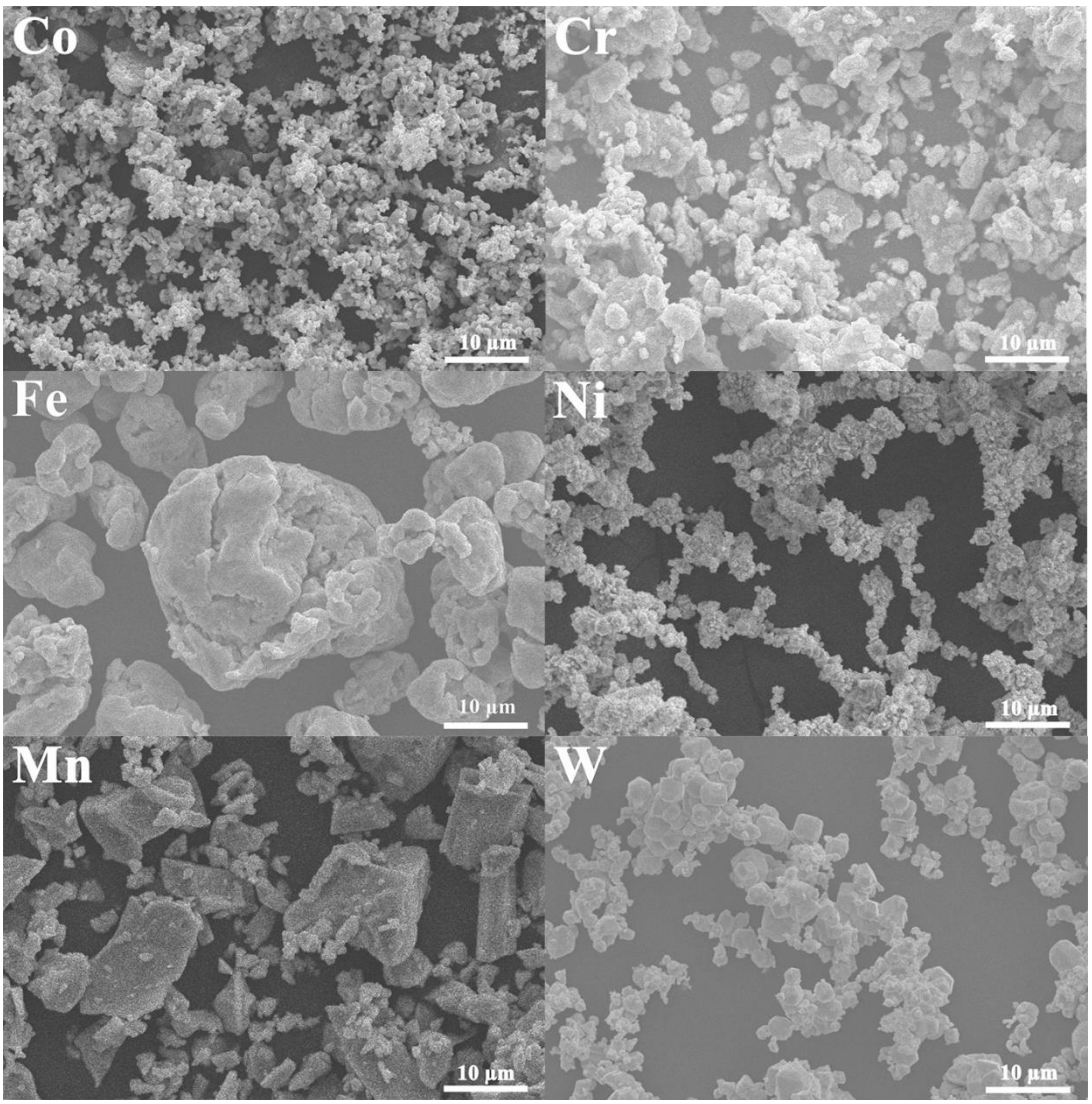

Figure 9. SEM images of as received Co, Cr, Fe, Ni, Mn and W powders.

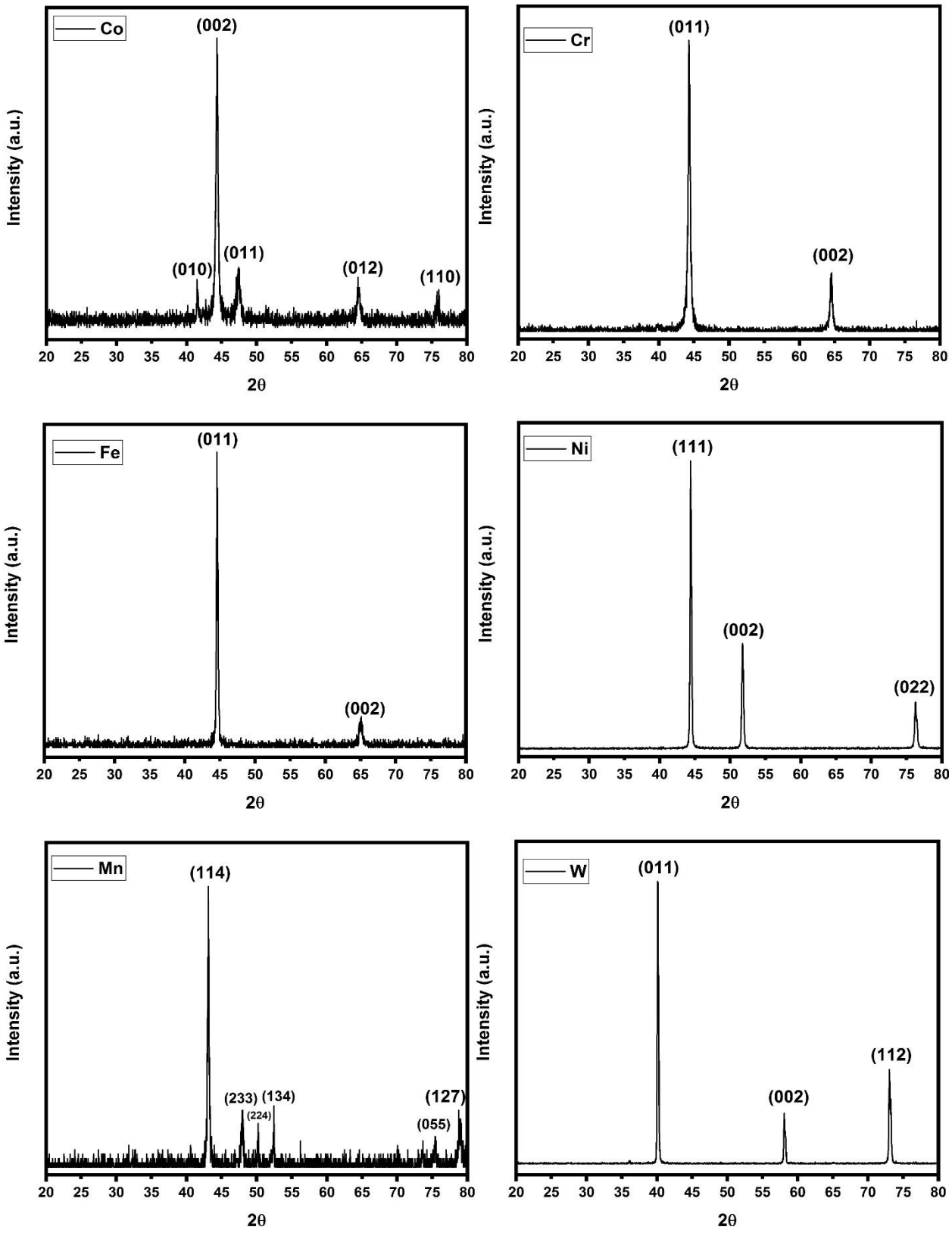

Figure 10. XRD patterns for as received Co, Cr. Fe, Ni, Mn and W elemental powders.

In figure 11 is presented the backscattered SEM image of pressure less sintered conventional W-Ni-Fe tungsten heavy alloy which is also the current industrial standard. In this figure W represents the tungsten particles while B represents the nickel iron binder matrix. This is a classic microstructure obtained after the liquid phase sintering of bi-phase composite [46], [47]. EDS analysis presented in figure 12 verifies the elemental composition of W-particles and binder phase matrix. XRD analysis presented in figure 13 shows characteristic peaks for bcc-tungsten particle and fcc crystal structure of Ni-Fe binder. These results are in accordance with the results reported by other researchers [47]–[49].

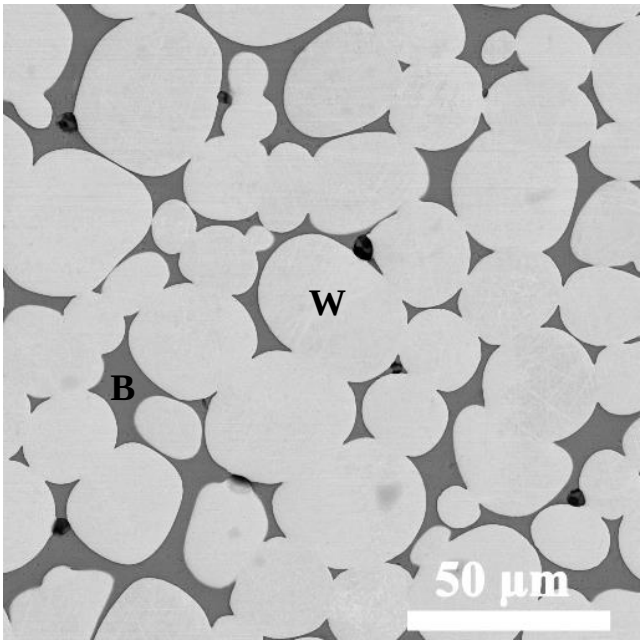

Figure 11. SEM micrograph of W-Ni-Fe

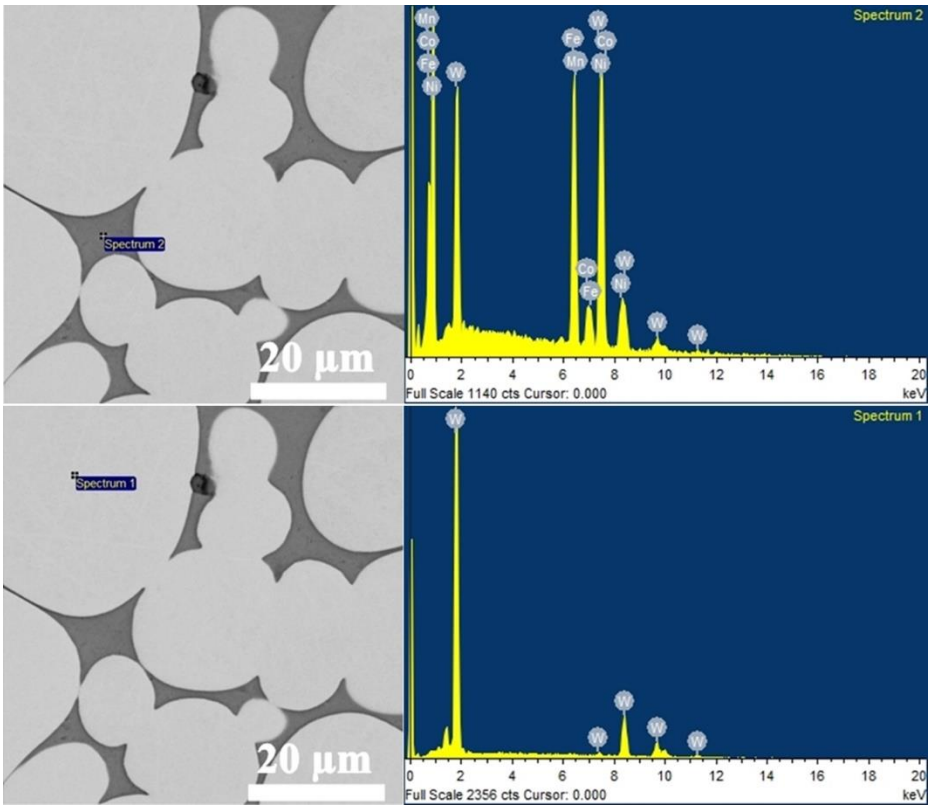

Figure 12. Spectrum 1 is the EDS result for particle region while, Spectrum 2 is the result for binder region.

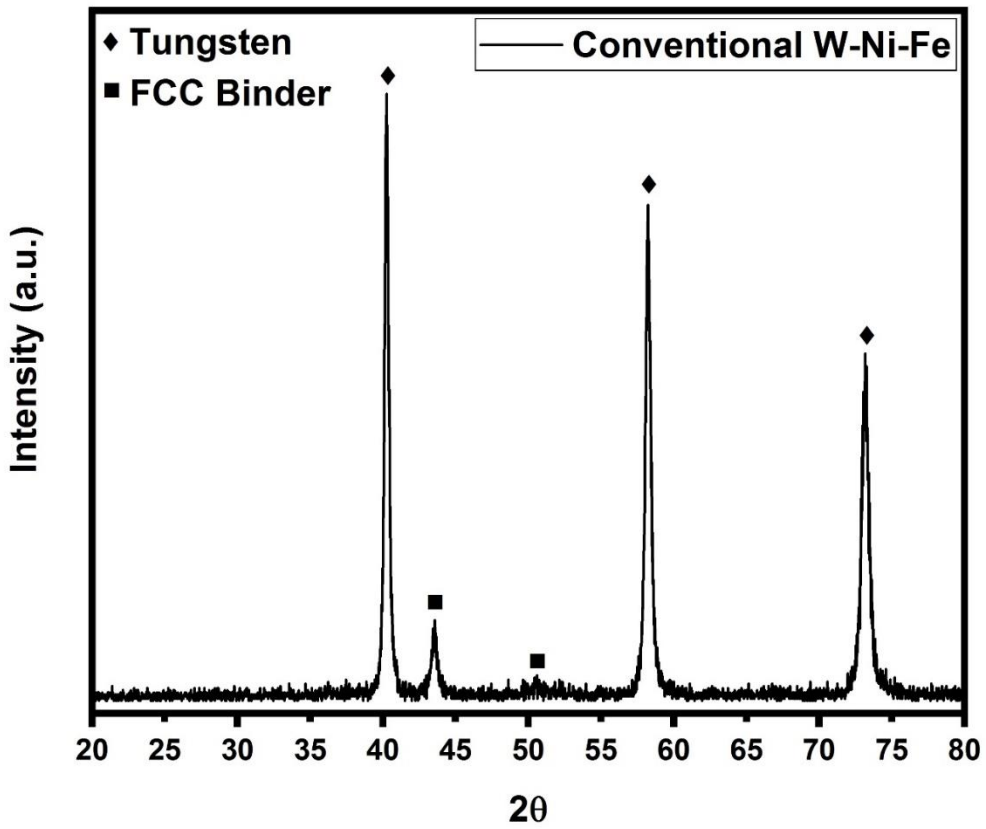

Figure 13. XRD pattern for pressure less sintered conventional

4.1.1 Pressure less sintering of W-HEA

In order to assess the possibility of manufacturing high entropy alloy-based tungsten heavy alloy through pressure less sintering. A green compact of (93W-7$CoCr_{0.75}FeNiMn$) powders was sintered under the same environment i.e. hydrogen gas and similar sintering conditions (figure 6 a) that are currently in use for conventional W-Ni-Fe (industrial standard). In figure 14 is presented the SEM micrograph for pressure less sintered W-HEA. The light areas (W) in the figure, are connected network of tungsten particles while the isolated grey areas (B) are binder matrix. While, the black regions represent discontinuities and porosities. The figure also indicates the presence elongated pores which is mainly due the entrapped gas inside the pores during coarsening process. The gas in this can be the water vapors which were generated as a result of reaction between hydrogen (present inside sintering furnace) and delay release of dissolved oxygen in tungsten particles [38], [50]. It can also be observed that, this microstructure is very different to the classic liquid phase sintered microstructure for conventional tungsten heavy alloy mentioned

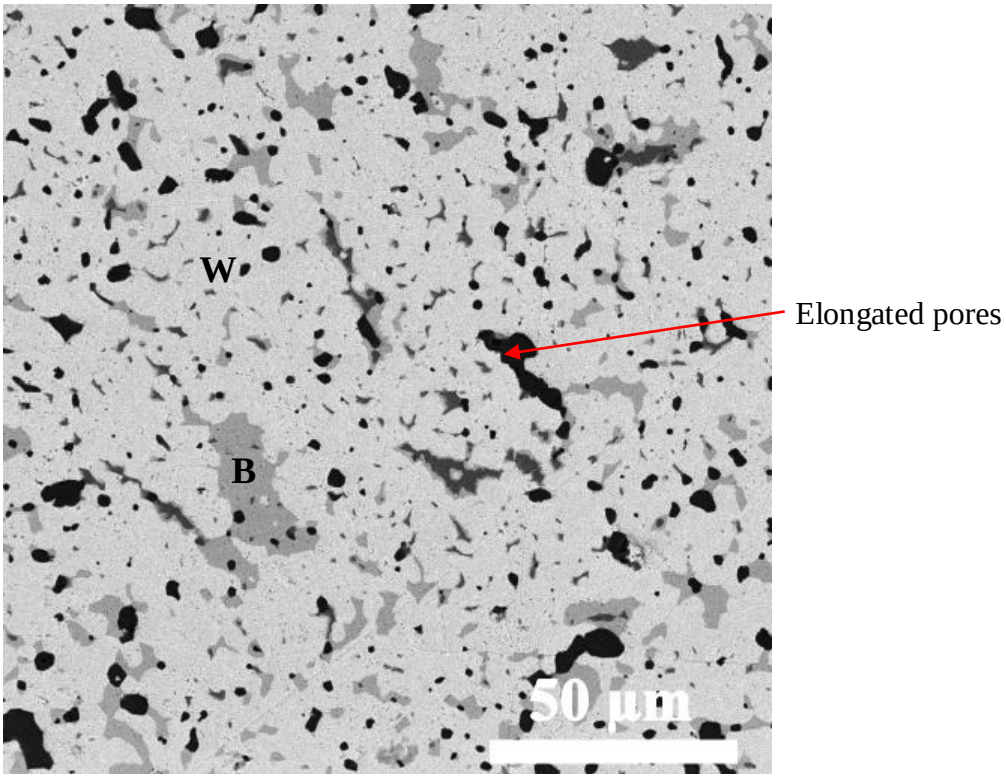

Figure 14. SEM micrograph of pressure less sintered W-HEA.

in figure 11. In order to explain the difference, it is pertinent to understand the stages involved in the liquid phase sintering. These stages are stated as below [51][52]:

1. Rearrangement
2. Solution-reprecipitation
3. Solid state sintering

4.1.1.1 Rearrangement

In the case where a mixture of powders is compacted, the solid particles undergo solid state sintering as the compact is progressively heated. In liquid phase sintering, the solute is generally soluble in liquid. As the liquid forms, it starts to dissolve and wet the solid particles. This liquid starts to penetrate in between the solid grains and thereby it starts to dissolve the solid-solid bonds at contact points, which were previously formed during heating of the compact. The driving force behind this whole process is reduction in the free energy; associated with solid particles. The liquid exerts capillary force on to the solid particles and therefore, densification start to happen at rapid pace. This process in which liquid starts to disintegrate the solid sintered grain by dissolving the contact points and densification starts is known as rearrangement.

4.1.1.2 Solution-reprecipitation

As the system progresses the inherent porosities are eliminated by lowering of surface energies. The compact, under the capillary action acts as a viscous solid and hence the process of densification slows down. In the second stage of liquid phase sintering which is known as solution-reprecipitation. Mass transport of solid particle takes place through liquid media by means of diffusion. The grain size distribution of solid particles creates a solubility gradient in which smaller particles tend to dissolve more rapidly than large ones. These small grains dissolve into the liquid and diffuse out to reprecipitate on the larger grains. Therefore, during this stage grain coarsening remains predominant; the coarsening of grains generates more wider spaces around grains which assist tighter packing hence, density of the system further increases.

4.1.1.3 Solid state sintering

This is the last stage of liquid phase sintering in which densification is relatively slower due to the presence of solid skeleton (W-W). The microstructure continues to get coarser by virtue of diffusion. During this stage, the pores also grow if they contain an entrapped gas moreover, the solid grain contacts accounts for solid state sintering. This last stage generally increases the W-W contact (contiguity) which results in inferior mechanical properties.

In view of the stages involved during the liquid phase sintering process, it is clearly evident that the binder was not able to rearrange the W particles and therefore, the solid-state bonds; formed during heating could not be dissolved or overcome by the

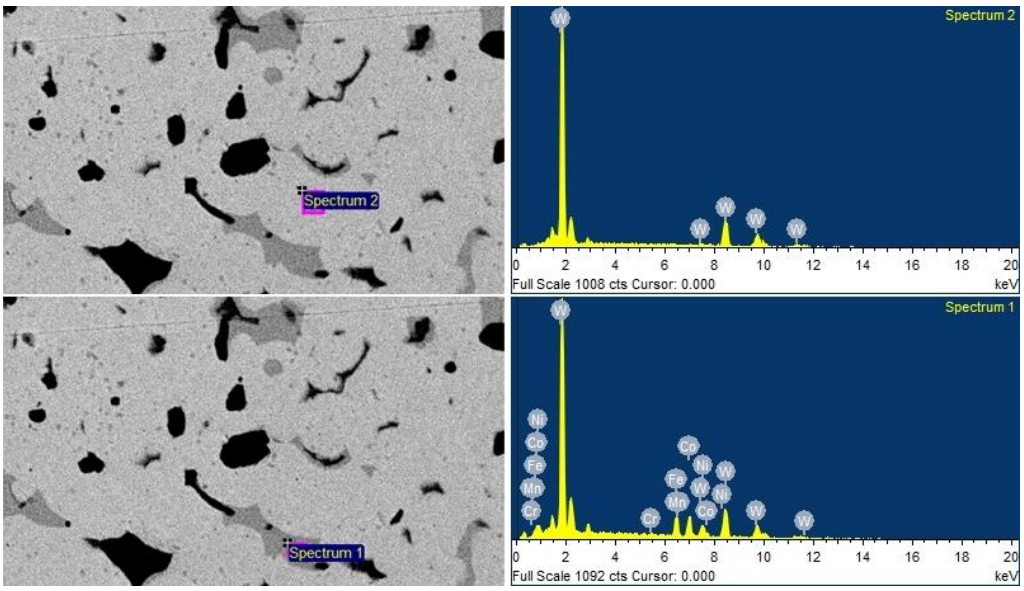

Figure 15. Spectrum 1shows the EDS result for particle region, Spectrum 2 shows the result for binder region.

liquid binder. However, the liquid at some places can be seen to have penetrated and thereby dissolved some proportions of tungsten particles and the same was supported by EDS analysis presented in figure 15 which shows the presence of dissolved tungsten inside binder matrix. Moreover, as stated by other researchers the binder did not show signs of non-wetting the tungsten particles which binders do by protruding from the surface or by causing swelling to the component [53]. Another factor which might have kept the liquid from rearrangement stage could be the inherent "sluggish diffusion effect" in high entropy alloys[54]. Therefore, a rather slower diffusion of liquid (binder) may have hindered the rearrangement and densification process. This microstructure contains a strong and very connected skeleton structure of tungsten which accounts for an extremely high contiguity. A high contiguity offers very inferior mechanical properties especially ductility and toughness. It is therefore, concluded that pressure less sintering did not suit the fabrication of W-HEA.

4.1.2 Hot Iso-static Pressing (HIP) sintering of W-HEA

The driving force behind sintering is minimizing the surface free energy of particles. The elimination of pores and densification are mainly carried out by the penetrating liquid and mass transfer through diffusion. However, in systems in which densification via diffusion is sluggish or ineffective, an external pressure at sintering temperature boosts the driving force which spur up the densification process. In HIP sintering, the powder compact is progressively heated under vacuum up to the sintering temperature; this heating results in solid to solid bonds formation known as pores closing. At sintering temperature when liquid forms, the compact is subjected to high external gas pressure; equally distributed in all directions similar to hydrostatic pressure state [55]. This liquid at high temperature and under pressure densifies the system by following the classical stages mentioned earlier in 4.1.1. In figure 16, is presented the backscattered electron SEM image for HIP sintered W-HEA. The round particles (W) are tungsten particles while light grey areas are of binder matrix (B). With external pressure liquid showed remarkable improvement in diffusion and the rearrangement process can be seen have taken place. The inherent polygonal shape of tungsten

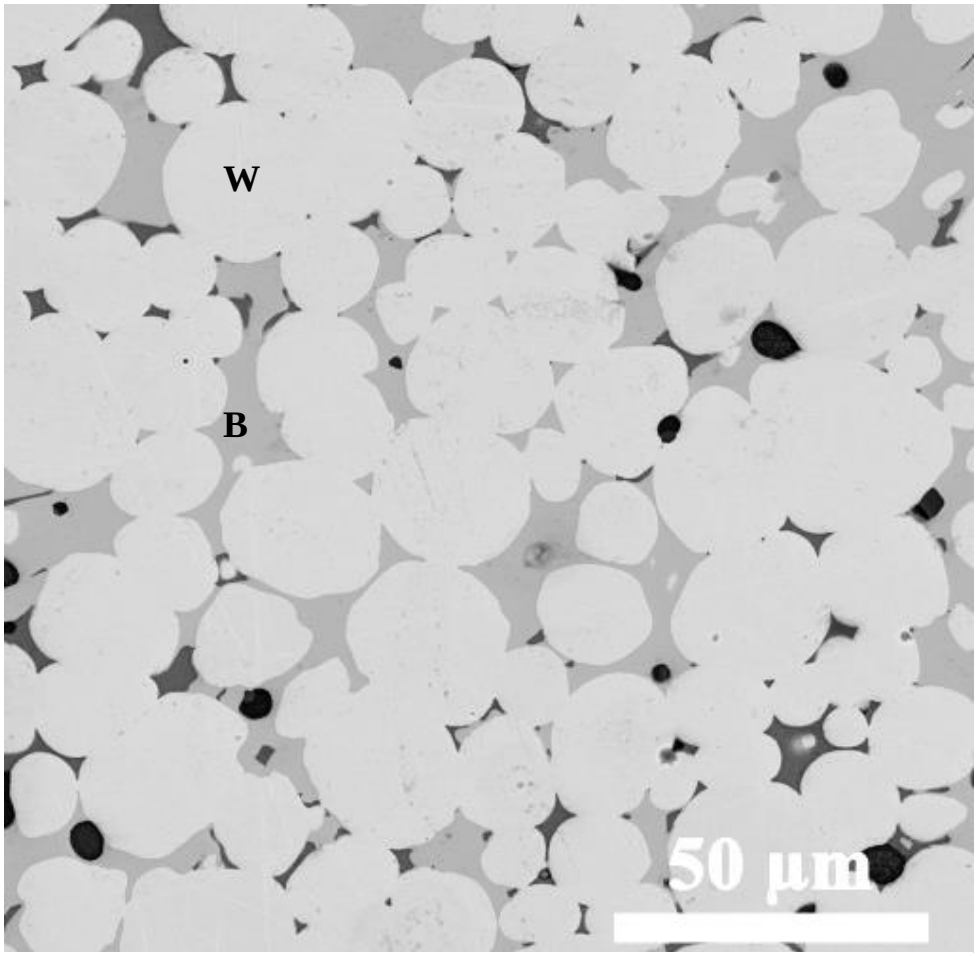

Figure 16. SEM micrograph of HIP sintered W-HEA

particles has been converted into round shape just like in conventional W-Ni-Fe. However, grain coarsening seems to be not up to the mark as one can see finer microstructure with small grains still present and ready to be dissolved and transported for reprecipitation on to the large ones. It is due to these undissolved small particles that optimum grain size accommodation could not took place and therefore, full densification could not be attained. Figure 17 represents the EDS analysis for particle and binder regions respectively. The EDS results were found to be similar to the pressure less sintered W-HEA which again proves that binder showed solubility for W however, a boost was required for liquid penetration and rearrangement of particles; which was provided by HIP. In figure 18 (a) is presented the XRD pattern for HIP sintered W-HEA. Similar to conventional W-Ni-Fe characteristic peaks of tungsten and binder are visible however, the decrease in absolute intensity of tungsten peaks indicated that, tungsten particles were more dissolved by the HEA binder than conventional Ni-Fe system [49]. The peak position for fcc-HEA binder are identical to the fcc-Ni-Fe system present in conventional tungsten heavy alloys. This proves the hypothesis that, in-situ manufacturing of HEA through conventional powder

metallurgy route is possible and practical. Moreover, Mn is prone to oxidation under high temperature and therefore, MnO peak can also be seen in the XRD diffractogram. MnO has the tendency to delimit the densification and therefore, discontinuities can be seen in the microstructure [56]. In figure 18 (b) the XRD plots for W-HEA and as received cobalt powder were drawn between 2θ (40˚-50˚). It is pertinent to note that, due to relatively larger quantity of tungsten powder the XRD peaks have been dominated by it therefore, we have to zoom so as to view the possibility of other peaks. In figure 18 (b) it can be seen that individual peaks of cobalt are present but in relatively lower intensities which means cobalt was not entirely involved in the bonding of HEA. Previously, it has been reported that cobalt has the tendency to segregate along grain boundaries and form intermetallic with tungsten [49].

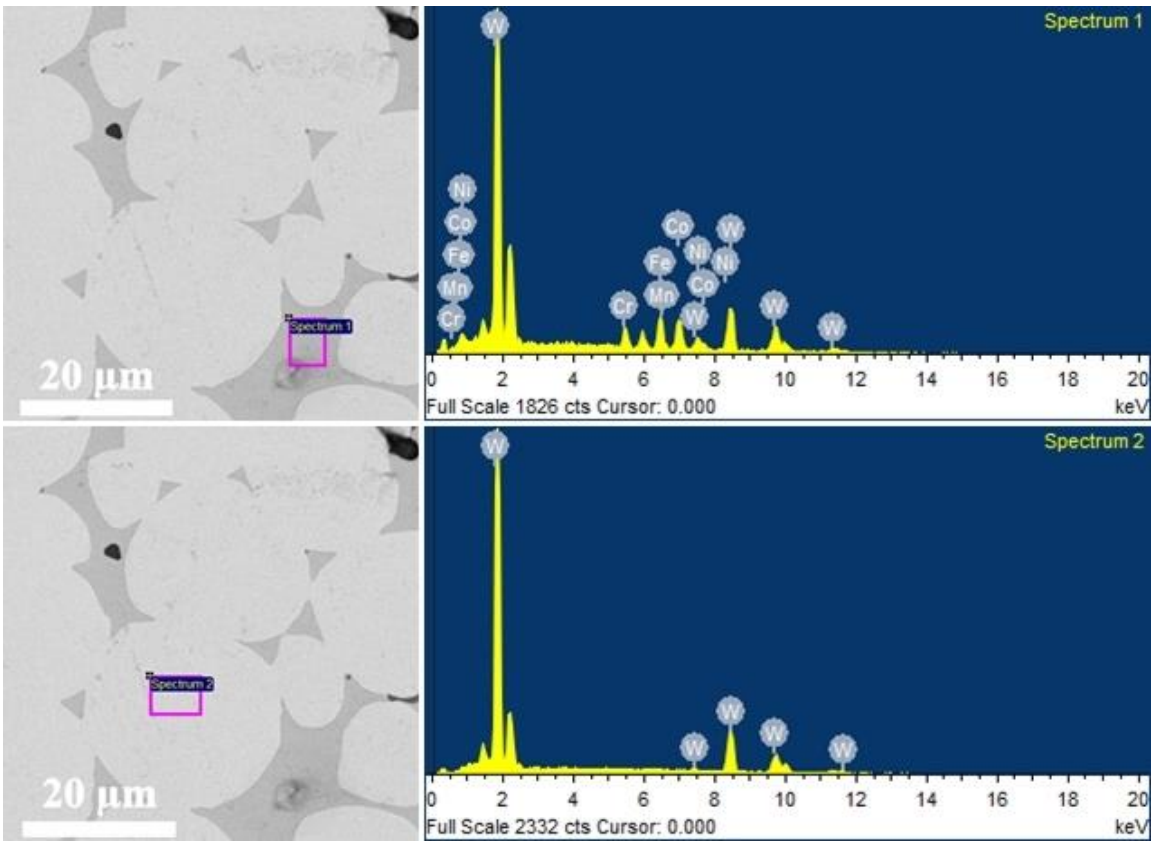

Figure 17. Spectrum 1 represents the EDS results of binder; Spectrum 2 represents the EDS results for particle.

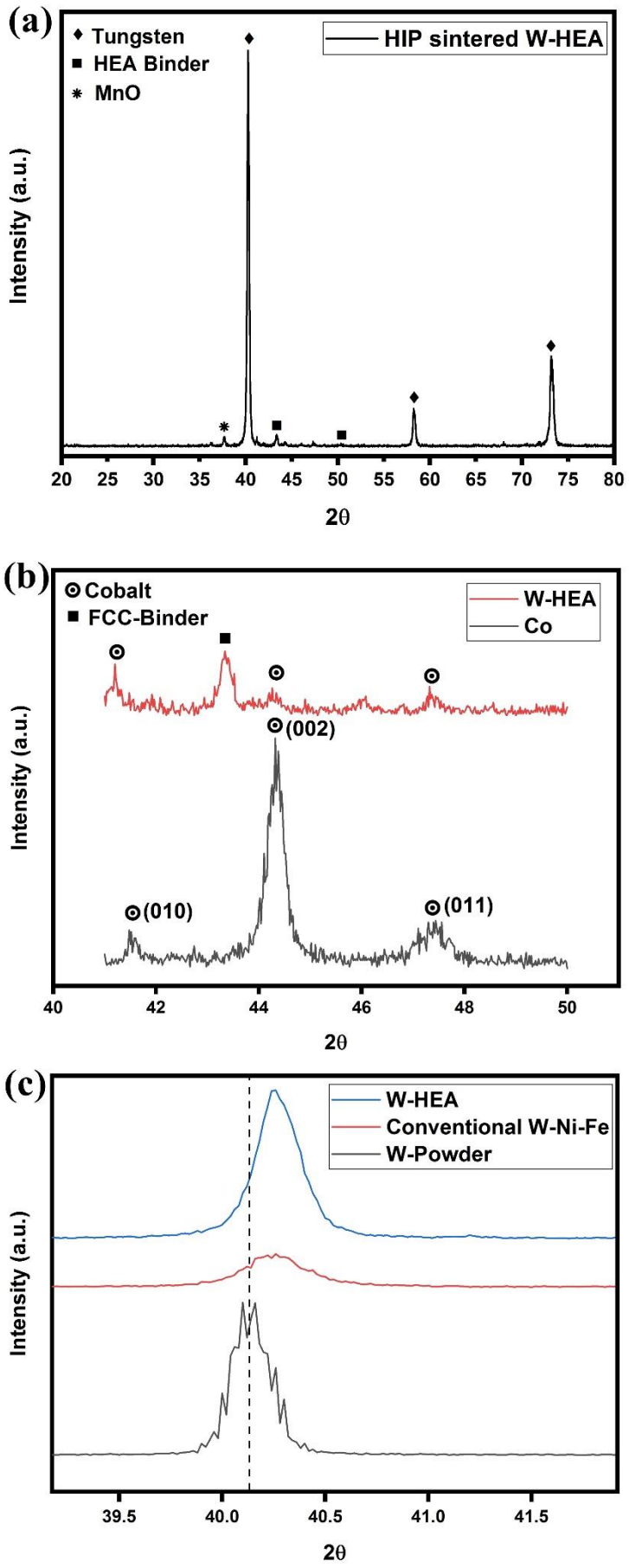

Figure 18. (a) XRD plot of HIP sintered W-HEA (b) XRD plots for Cobalt powder and W-HEA (c) XRD plots for W-powder, conventional W-Ni-Fe and W-HEA; shift in peaks can be observed for both composites.

Nickel and iron are the chief ingredients which boost solubility of tungsten into the liquid phase meanwhile cobalt acts as a restrainer [49]. The lower absolute intensity of tungsten accounts for the fact that the presence of nickel and iron in equally molar ratio have resulted in dissolving more tungsten than they usually do in a 4Ni:3Fe conventional tungsten heavy alloy system.

In figure 18 (c) XRD plots for tungsten powder, conventional W-Ni-Fe and HIP sintered W-HEA are shown. It can be seen the tungsten peaks are shifted towards right side or towards higher 2θ value for both the conventional and W-HEA composites. This is due to the decrease in interplanar spacing and lattice parameter of tungsten due to solid solution formed during the solution reprecipitation stage. In W-HEA the peak shift is slightly greater than conventional tungsten heavy alloy.

4.1.3 Particle size analysis

Particle size plays a vital role in determining the final mechanical properties of composites, it is therefore pertinent to analyze the particle size in conventional tungsten heavy alloys (W-Ni-Fe) and W-HEA. Particle size distribution was calculated through an image processing software ‘image J’ and in figure 19 (a) is presented the particle distribution for conventional W-Ni-Fe and in figure 19 (b) the same is presented for W-HEA.

The mean particle size for W-Ni-Fe was found to be 20.86 μm while for W-HEA it was found to be 16.13 μm, which means that W-HEA has a finer microstructure than conventional W-Ni-Fe. In figures 19 (a) and (b) are presented the values of standard deviation (S.D.) for both conventional and high entropy alloy-based tungsten heavy alloys. It can be seen the S.D. value for conventional W-Ni-Fe is high at 8.072 than; for the W-HEA which is 5.55. The higher value of S.D. indicates the existence of unequal particles inside composite, which indicates that system underwent grain growth during the last stage of liquid state sintering whereby grain coarsening takes place at the cost of smaller ones. A distribution of small and coarse grain sizes accounts for high S.D. value for conventional heavy alloys. On the other hand, in W-HEA the smaller and similar particles result in a finer microstructure. There are possibly two reasons for the finer structure in W-HEA; one, that the grain growth during the last stage of liquid phase sintering was slower owing to the sluggish diffusion affect in high entropy alloys and two, the presence of higher percentage of cobalt have hindered

the solution reprecipitation stage during the liquid phase sintering of W-HEA. Cobalt usually acts a grain refiner and as the XRD results suggests cobalt retained its peaks and might have segregated along the grain boundaries. Hence, nickel and iron were able to dissolve tungsten particles during the rearrangement stage but cobalt restraint the reprecipitation of tungsten and thus affected the swift mass transfer through liquid phase; thus, rendering a finer microstructure.

4.1.4 Contiguity in liquid phase sintered composites

Contiguity is an important microstructure parameter which is quantitative, and its value has a pronounced effect on the mechanical properties of tungsten heavy alloys. Contiguity is basically a measure of inter-particle or interphase contact in a composite and therefore, it can be calculated by mathematical means [57]. In this work the line

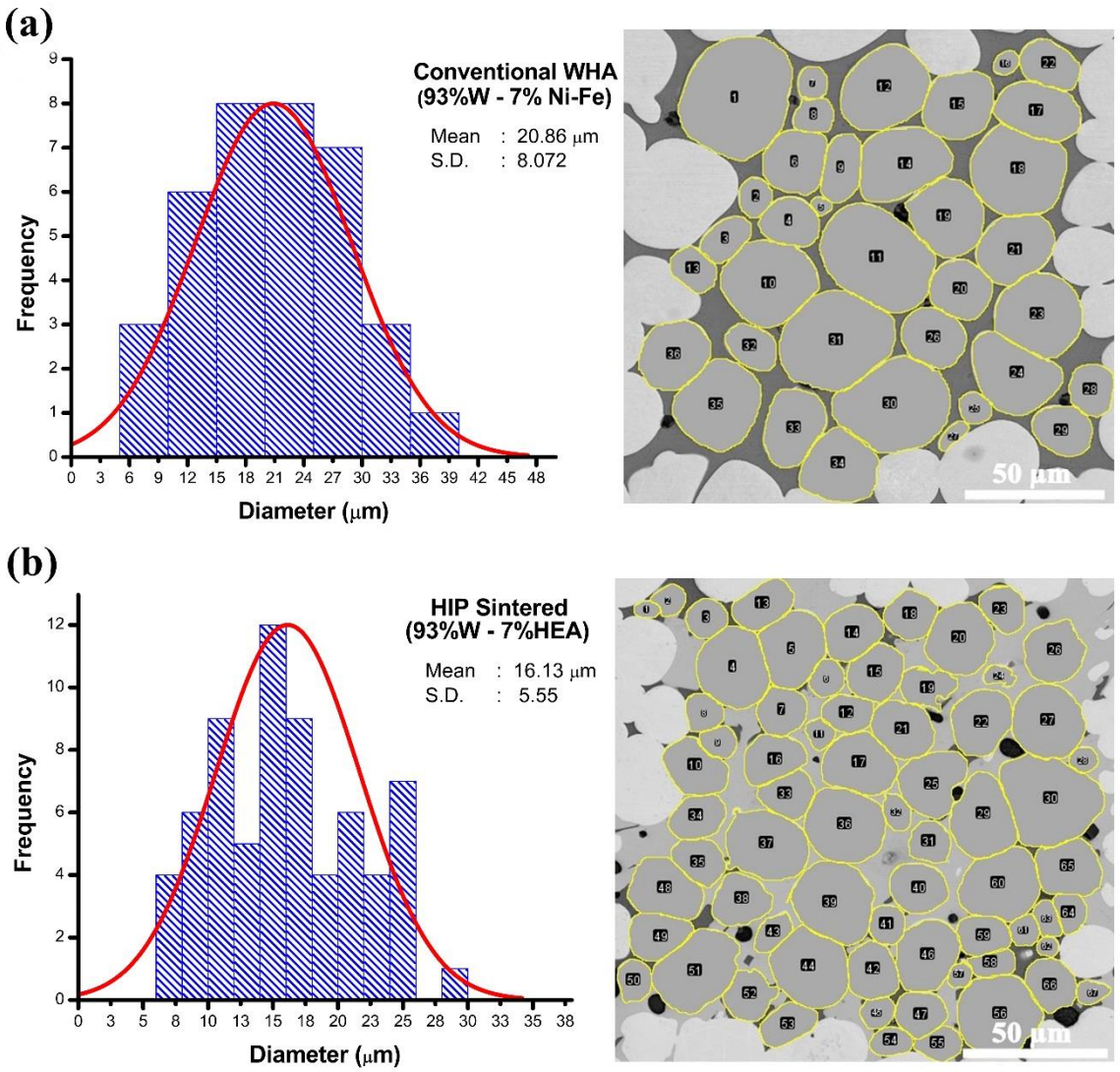

Figure 19. Particle size distribution for (a) conventional W-Ni-Fe (b) HIP sintered W-HEA

intercept method was used to calculate the contiguity for both conventional and high entropy alloy-based tungsten heavy alloys. Following is presented the formula for calculating the contiguity in liquid phase sintered tungsten heavy alloys:

$$\mathbf{C_W = 2N_{WW} / (2N_{WW} + 2N_{WB})} \text{ ..... } \mathbf{(5)}$$

Where,

C_W = Contiguity of Tungsten.

N_{WW} = No. of tungsten to tungsten interfaces per unit length of drawn line.

N_{WB} = No. of tungsten to binder interfaces per unit length of drawn line.

Contiguity was measured with the help of an image processing software 'image J' and in figure 20 (a) and (b) are presented the line intercepted SEM micrographs of conventional and W-HEA heavy alloys respectively and results are presented in table 4-1.

Table 4-1. Contiguity values for conventional and W-HEA.

Samples	**Contiguity**
Conventional W-Ni-Fe	0.34
W-HEA	0.42

Although, W-HEA have finer microstructure but it has a higher contiguity value than conventional W-Ni-Fe, which means that in W-HEA the tungsten particles are in more contact and rather less separated by the binder matrix. The separation or lowering in contacts of particles is generally carried out during the solution reprecipitation and grain growth stages of liquid phase sintering and as discussed earlier that the presence of cobalt have not only provided the finer microstructure but has also hindered the W-HEA to attain low contiguity value through effective mass transfer and grain growth.

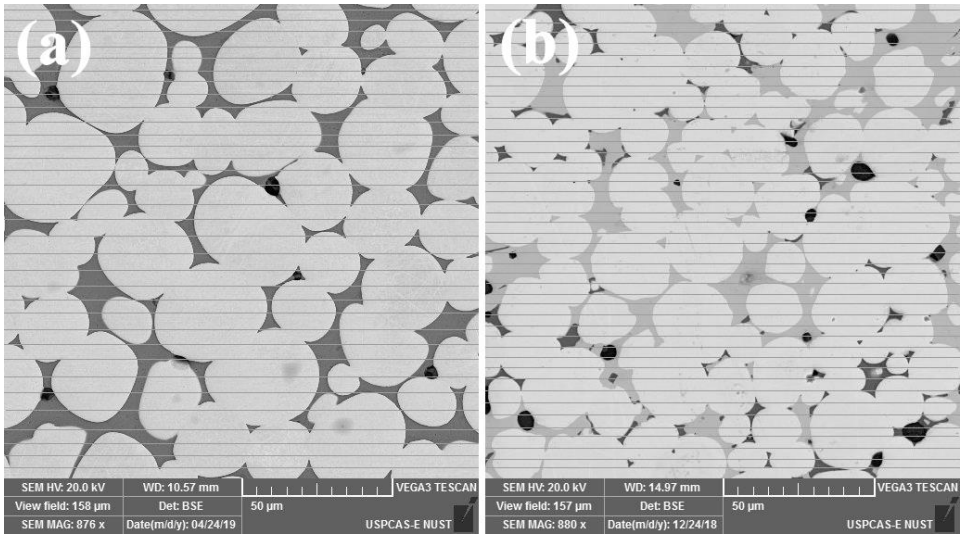

Figure 20. Line intercepted SEM images for calculation of contiguity in (a) Conventional W-Ni-Fe and (b) HIP sintered W-HEA.

4.1.5 Densities of conventional and W-HEA tungsten heavy alloys.

Densities of both composites were measured through Archimedes water immersion technique and the results are presented in table 4-2 below:

Table 4-2. Densities of conventional and W-HEA.

Samples	Density (g/cm^3)
Conventional W-Ni-Fe	17.65
W-HEA	17.40

Densification in liquid phase sintered composites is completed during the all three stages of sintering, and therefore it can be seen that due to hinderance in the mass transfer, sluggish diffusion and grain growth the W-HEA lagged behind the conventional industrial standard in attaining a higher or equal value of density. Moreover, MnO have been reported to delimit the densification of heavy alloys and generates discontinuities (pores) [56]. The presence of Mn in relatively higher quantity than conventional W-Ni-Fe could also be the reason for lower W-HEA density than the conventional one.

4.1.6 Impact testing

Unnotched Charpy impact testing of both samples were conducted according to the ASTM-B-925 standard. Both samples were found to be machinable and therefore the image of impact testing sample is presented in figure 21 while the results are presented in table 4-3.

Table 4-3. Unnotched Charpy Impact testing results for W-Ni-Fe and W-HEA.

Samples	Energy (J)
Conventional W-Ni-Fe	25
W-HEA	6

The higher contiguity in W-HEA, resulted in an inferior impact energy profile; lagging far behind the conventional W-Ni-Fe. Moreover, lower densification results in more discontinuities which deleteriously affect the toughness of composites and that case is visible for W-HEA.

4.1.7 Hardness testing

Micro Vickers hardness testing for conventional and W-HEA were conducted on 0.1 kgf and 1.0 kgf, respectively and the corresponding values are shown in table 4-4. In figure 22 are presented the micro indentations (0.1 kgf) for the W-Ni-Fe and W-HEA.

As was discussed in the XRD results, the absolute intensity of tungsten in W-HEA was found to be lesser than conventional W-Ni-Fe system, which accounts for greater initial solubility of tungsten in the presence of nickel and iron however, due to hinderance from cobalt during the solution reprecipitation stage the dissolved tungsten was not able to effectively reprecipitate on to the W grains and undergo grain growth. It is due to this reason that, tungsten particles in W-HEA underwent solid solution strengthening and therefore shows higher hardness values than conventional ones. The binder matrix in W-HEA has been found to be harder than the conventional Ni-Fe alloy. The overall hardness of W-HEA was found to be greater than W-Ni-Fe. Cobalt

Figure 21. Machined unnotched Charpy impact testing sample of HIP sintered W-HEA

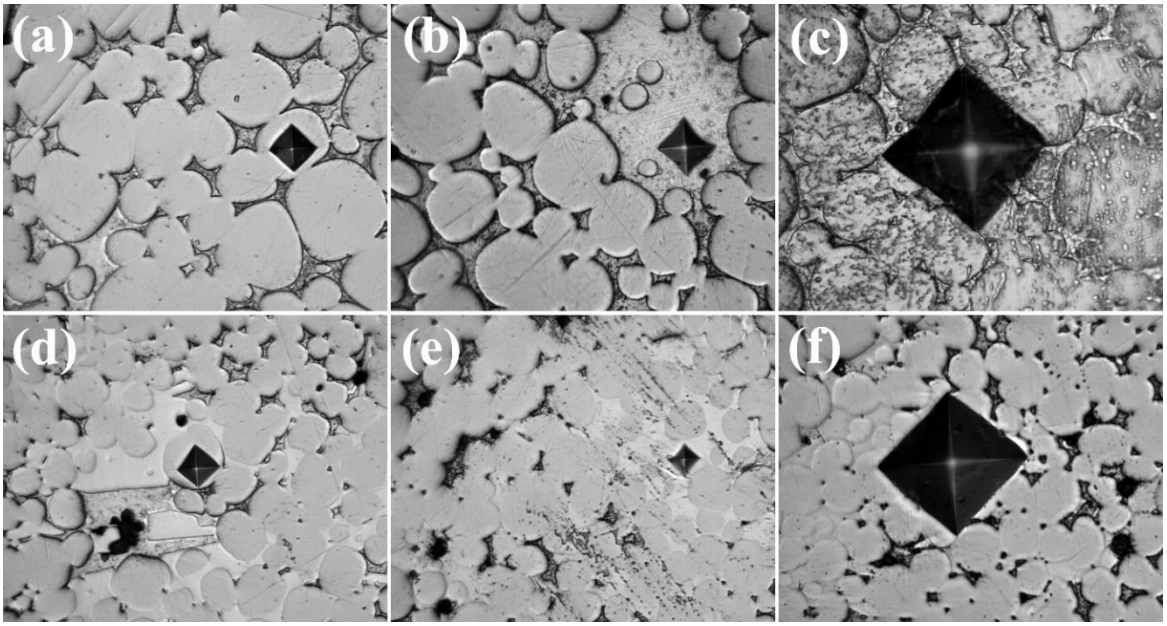

Figure 22. Micrographs representing indenting impressions for Vickers hardness test (a) 0.1 Kgf on W-particle for conventional W-Ni-Fe (b) 0.1 Kgf for binder region in conventional W-Ni-Fe (c) 1.0 Kgf for conventional W-Ni-Fe.

segregated along the tungsten grains causes embrittlement and that could be the main cause for raising the hardness of W-HEA [49].

Table 4-4. Vickers hardness for conventional and W-HEA.

Sample	**Vickers Hardness**		
	HV/0.1		**HV/1.0**
	W Particle	**Binder**	**-**
Conventional	398.37	261.08	322.00
W-HEA	528.14	765.77	456.75

4.1.8 Compression testing

Compression testing as per ASTM B-925 (strain rate 0.005 in/in.min) was conducted on samples with following specifications:

Diameter = 13.5 mm

Length = 9 mm

L/D ration = 1.5

Figure 23 (a) and (b) shows the fractured samples after compression testing, the fracture line for conventional W-Ni-Fe is rather smooth which accounts for a ductile fracture, whereas the roughly cracked surface of W-HEA shows that the fracture was brittle. Moreover, in figure 24 the stress-strain curves show that W-Ni-Fe underwent plastic deformation but W-HEA showed a very small deformation, so as the case in

the final length of the two different tungsten heavy alloys (figure 23). Table 4-5 compares the values of ultimate strength, modulus and yield strength, conventional heavy alloy because of higher density and less contiguity showed better mechanical profile. While W-HEA, owing to discontinuities and high contiguity underwent triaxial stress which caused the brittle fracture.

As evident from previous characterization results, the W-HEA contains cobalt which causes embrittlement by segregating along the grain boundaries; moreover, it also hindered the full densification process during sintering which left discontinuities. These discontinuities act as stress raiser and crack initiators which travel along embrittled grain boundaries to leave a brittle fracture. The lower toughness value obtained through unnotched Charpy test is also in accordance with the compression test.

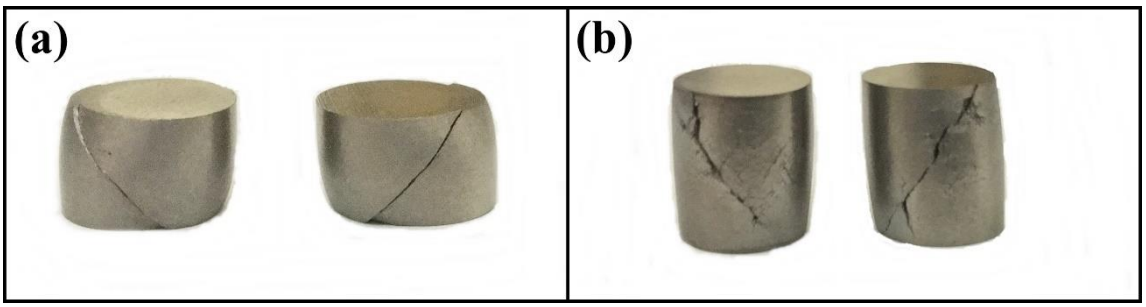

Figure 23. Fractured samples after compression testing (a) Conventional W-Ni-Fe (b) HIP

Table 4-5. Compression testing results for W-HEA and Conventional W-Ni-Fe.

Sample	**Compression Testing**		
	Ultimate strength (MPa)	**Modulus (MPa)**	**0.2% Yield Strength (MPa)**
W-HEA	1788	26600	972
Conventional	2250	32500	1005

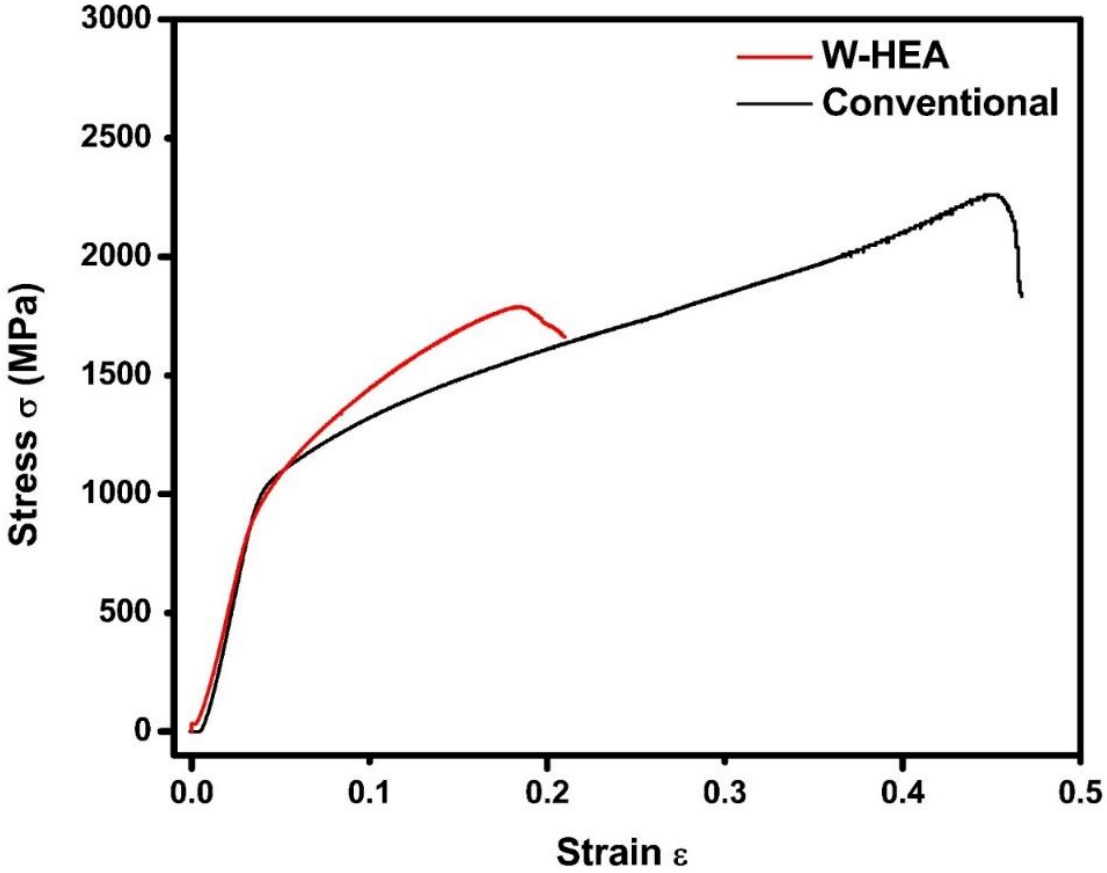

Figure 24. Compression testing of conventional W-Ni-Fe and W-HEA alloys.

Conclusions

- Conventionally, the tungsten heavy alloys were manufactured through liquid phase sintering of powders containing 80-98% W and remainder binder matrix containing Ni, Fe, Co, Mn or some other alloying elements.
- High entropy alloys are a new class of materials which require five or more principle elements and have been reported to offer outstanding properties.
- CoCrFeNiMn high entropy alloy was reported to offer better properties as binder matrix than conventional binder, Cobalt in tungsten carbides.
- However, no previous efforts were made in exploring the in-situ manufacturing of high entropy alloys through powder metallurgy route.
- Keeping in view the ongoing practice of manufacturing WHA with a binder; containing up to four elements, it was encouraging to study the possibility of manufacturing W-HEA through conventional manufacturing routes.
- All powders i.e. W, Co, Cr, Fe, Ni and Mn were mixed, pressed and set for liquid phase sintering under pressure-less sintering.
- Under pressure-less sintering the liquid formed was unable to rearrange the tungsten particles and penetrate through the solid skeleton of W-W particles. Hence, it did not give the desired microstructure.
- In HIP sintering, under high temperature and high argon pressure the liquid was able to penetrate through the W-W network and thus classic liquid phase sintered microstructure was obtained.
- SEM/EDS and XRD results verifies the formation of fcc HEA binder among rounded tungsten particles.
- However, the XRD results showed the presence of unreactive cobalt and presence of MnO. Co has the tendency to segregate along grain boundaries and cause embrittlement, while MnO delimits the full densification which imparts pores or discontinuities inside the sintered composite.
- The mechanical testing of W-HEA was conducted and the results were compared with the conventional W-Ni-Fe.
- It was found that, W-HEA is brittle and lack the desired toughness and strength.
- High contiguity, incomplete densification and presence of cobalt along tungsten grain boundaries resulted in lowering the mechanical profile of the W-HEA composite.

- It is therefore, concluded that in-situ manufacturing of high entropy alloy is possible, however the oxidation of Mn at high temperature affected the full densification and presence of cobalt along grain boundaries imparted embrittlement to W-HEA.

Recommendations

- A pre-alloyed or pre-formed high entropy alloy (mechanical alloying) could be used as binder for liquid phase sintering of tungsten heavy alloy, as in-situ formation of HEA allows the pure particles to react with oxygen; which is inherently present inside tungsten particles.
- Moreover, considering the vast flexibility in choice of elements for high entropy alloy one can try different elements other than cobalt and manganese, which have high solubility for tungsten.

Annexure

Calculations of Atomic Weight and Weight Percentages[58]

From wt% to at%

First, we must consider weight in terms of grams. To do this, consider a 100 grams sample of the alloy. For example, 100g of Fe-7wt%C contains 7g of Carbon and 93g of Iron.

Atomic weight of Fe is 56

Atomic weight of C is 12

Avogadro's Number is 6.022×10^{23}

Number of atoms in 7 grams of Carbon

= 7 x Avogadro's Constant / atomic weight of C

$= 7 \times 6.022 \times 10^{23} / 12$

$= 3.513 \times 10^{23}$

Similarly, number of atoms in 93 grams of Iron

= 93 x Avogadro's Constant / atomic weight of Fe

$= 93 \times 6.022 \times 10^{23} / 56$

$= 10.000 \times 10^{23}$

Therefore, at% of Carbon

= C atoms x 100% / (total of C + Fe atoms)

$= 3.513 \times 10^{23} \times 100 / (3.513 + 10.000) \times 10^{23}$

= 26%

So, Fe-7wt%C is equivalent to Fe-26at%C

From at% to wt%

Cementite forms at Fe-25at%C. At what weight percent is this?

Consider a sample containing 100 atoms. For example, a sample of Fe-25at%C would contain 25 Carbon atoms and 75 Iron atoms.

Weight of 25 C atoms

= 25 x atomic weight of C / Avogadro's Constant

= 4.98 atomic mass units

Weight of 75 Fe atoms

= 75 x atomic weight of Fe / Avogadro's Constant

= 69.74 atomic mass units

Therefore, wt% of Carbon

= C weight x 100% / (total weight of C + Fe atoms)

= 4.98 x 100 / (4.98 + 69.74)

= 6.66%

So, 25at%C is equivalent to 6.66wt%C”

References

[1] A. Arora, "Tungsten Heavy Alloy For Defence Applications," *Mater. Technol.*, vol. 19, no. 4, pp. 210–216, **2004**.

[2] Y. Şahin, "Recent Progress in Processing of Tungsten Heavy Alloys," *J. Powder Technol.*, vol. 2014, **2014**.

[3] Erik Lassner and Wolf-Dieter Schubert, *Tungsten*, First. New York: Springer Science+Business Media, LLC, **1999**.

[4] R. Warke, "of Material Tsughrw s , Thermal Shock Resistance , and Microstructure of High Tungsten , Silver-Tungsten omposite Materials," **1975**.

[5] Suk-Joong L.Kang, "Sintering Densification,Grain Growth,and Microstructure," *Elsevier Butterworth-Heinemann Linacre House*, no. ISBN 978-0-7506-6385-4., pp. 9–18, **2005**.

[6] A. Upadhyaya, "Processing strategy for consolidating tungsten heavy alloys for ordnance applications," *Mater. Chem. Phys.*, vol. 67, no. 1–3, pp. 101–110, **2001**.

[7] J. Das, U. R. Kiran, A. Chakraborty, and N. E. Prasad, "Hardness and tensile properties of tungsten based heavy alloys prepared by liquid phase sintering technique," *Int. J. Refract. Met. Hard Mater.*, vol. 27, no. 3, pp. 577–583, **2009**.

[8] B. Dodd and Y. Bai, *Adiabatic Shear Localization*, Second. Massachusetts: Elsevier Ltd., **2012**.

[9] J. Mescall and V. Weiss, *Material Behavior Under High Stress and Ultrahigh Loading Rates*. New York: Plenum Press, **1983**.

[10] J. George E. Dieter, *Mechanical Metallurgy*, First. New York: McGraw-Hill Company, Inc., **1961**.

[11] Sidney H. Avner, *Introduction to Physical Metallurgy*, Second. New Dehli: Tata McGraw Hill Education Private Limited, **1997**.

[12] A. Lawley, "Modern Powder Metallurgy Science and Technology," *J. Met.*, pp. 15–25, **1986**.

[13] C. M. Lewandowski, N. Co-investigator, and C. M. Lewandowski, *Powder Metal Technologies and Applications*, vol. 7. **2015**.

[14] G. Randall M, *Powder Metallurgy Science*, Second. Princeton: MPIF, **1994**.

[15] T. F. By, T. H. E. Russian, and T. A. R. E. By, *Powder*, First. London: Pergamon Press Ltd, **1965**.

[16] D. G. R. William D. Callister, Jr., *Materials Science and Engineering*, 9th ed. Wiley, **2013**.

[17] S. J. Park, J. M. Martin, J. E. Guo, J. L. Johnson, and R. M. German, "Grain growth behavior of tungsten heavy alloys based on the master sintering curve concept," *Metall. Mater. Trans. A Phys. Metall. Mater. Sci.*, vol. 37, no. 11, pp. 3337–3346, **2006**.

[18] R. M and German, *Liquid Phase Sintering*, vol. 53, no. 9. **2013**.

[19] F. C. Cambell, *Elements of Metallurgy and Engineering Alloys*, First. ohio: ASM, **2008**.

[20] B. Cantor, I. T. H. Chang, P. Knight, and A. J. B. Vincent, "Microstructural development in equiatomic multicomponent alloys," *Mater. Sci. Eng. A*, vol. 375–377, no. 1-2 SPEC. ISS., pp. 213–218, **2004**.

[21] J. W. Yeh, "Alloy design strategies and future trends in high-entropy alloys," *Jom*, vol. 65, no. 12, pp. 1759–1771, **2013**.

[22] M.-H. Tsai and J.-W. Yeh, "High-Entropy Alloys: A Critical Review," *Mater. Res. Lett.*, vol. 2, no. 3, pp. 107–123, **2014**.

[23] S. R. B.S. Murty, J.W. Yeh, *High Entropy Alloys*, First. London, Oxford, Amsterdan, MA, San Diego: Elsevier Inc., **2014**.

[24] B. Cantor, "Multicomponent and high entropy alloys," *Entropy*, vol. 16, no. 9, pp. 4749–4768, **2014**.

[25] J. W. Yeh *et al.*, "Nanostructured high-entropy alloys with multiple principal elements: Novel alloy design concepts and outcomes," *Adv. Eng. Mater.*, vol. 6, no. 5, pp. 299-303+274, **2004**.

[26] C. Zhang and M. C. Gao, *CALPHAD modeling of high-entropy alloys*. **2016**.

[27] S. Guo, Q. Hu, C. Ng, and C. T. Liu, “More than entropy in high-entropy alloys: Forming solid solutions or amorphous phase,” *Intermetallics*, vol. 41, no. Supplement C, pp. 96–103, **2013**.

[28] S. GUO and C. T. LIU, “Phase stability in high entropy alloys: Formation of solid-solution phase or amorphous phase,” *Prog. Nat. Sci. Mater. Int.*, vol. 21, no. 6, pp. 433–446, **2011**.

[29] Y. Zhang, Y. J. Zhou, J. P. Lin, G. L. Chen, and P. K. Liaw, “Solid-Solution Phase Formation Rules for Multi-component Alloys,” *Adv. Eng. Mater.*, vol. 10, no. 6, pp. 534–538, **Jun. 2008**.

[30] C. T. Liu and J. O. Stiegler, “Ductile Ordered Intermetallic Alloys,” *Science (80-.).*, vol. 226, no. 4675, p. 636, **Nov. 1984**.

[31] S. Guo, C. Ng, J. Lu, and C. T. Liu, “Effect of valence electron concentration on stability of fcc or bcc phase in high entropy alloys,” *J. Appl. Phys.*, vol. 109, no. 10, **2011**.

[32] Y. Zhang, S. Guo, C. T. Liu, and X. Yang, “High-Entropy Alloys,” **2016**.

[33] S. Guo, C. Ng, J. Lu, and C. T. Liu, “Effect of valence electron concentration on stability of fcc or bcc phase in high entropy alloys,” *J. Appl. Phys.*, vol. 109, no. 10, p. 103505, **May 2011**.

[34] J. W. Yeh, “Recent progress in high-entropy alloys,” *Ann. Chim. Sci. des Mater.*, vol. 31, no. 6, pp. 633–648, **2006**.

[35] D. a. Porter and K. E. Easterling, *Phase Transformations in Metals and Alloys*. **1992**.

[36] R. M. German, *Sintering Theory and Practice*. New York: Wiley, **1996**.

[37] R. M. German, A. Bose, and S. S. Mani, “Sintering time and atmosphere influences on the microstructure and mechanical properties of tungsten heavy alloys,” *Metall. Trans. A*, vol. 23, no. 1, pp. 211–219, **1992**.

[38] R. M. German and K. S. Churn, “SINTERING ATMOSPHERE EFFECTS ON THE DUCTILITY OF W-Ni-Fe HEAVY METALS.,” *Metall. Trans. A, Phys. Metall. Mater. Sci.*, vol. 15 A, no. 4, pp. 747–754, **1984**.

[39] W. G. J. Northcutt, “Fabrication development of tungsten alloy penetrators.” **1976**.

[40] K. T. Ramesh and R. S. Coates, “Microstructural Influences on the Dynamic Response of Tungsten Heavy Alloys,” vol. 23, no. September, pp. 2625–2630, **1992**.

[41] B. H. Rabin and R. M. German, “Microstructure Effects on Tensile Properties of Tungsten-Nickel-Iron Composites,” vol. 19, no. June, **1988**.

[42] J.-W. Noh, E.-P. Kim, H.-S. Song, W.-H. Baek, K.-S. Churn, and S.-J. L. Kang, “Matrix Penetration of W/W-Grain Boundaries and Its Effect on Mechanical Properties of 93W-5.6Ni-1.4Fe Heavy Alloy,” *Metall. Trans. A*, vol. 24, no. November, pp. 2411–2416, **1993**.

[43] D. K. Kim, S. Lee, and H. S. Song, “Effect of tungsten particle shape on dynamic deformation and fracture behavior of tungsten heavy alloys,” *Metall. Mater. Trans. A Phys. Metall. Mater. Sci.*, vol. 29, no. 13, pp. 1057–1069, **1998**.

[44] S. Guha, C. Kyriacou, J. C. Withers, R. O. Loutfy, G. T. Gray, and R. J. Dowding, “Processing and Properties of Tungsten Heavy AUoys with Ni48Al12Fe40 Inteimetallic Matrix,” *Mater. Manuf. Process.*, vol. 9, no. 6, pp. 1163–1187, **Nov. 1994**.

[45] B. Cantor, *High-Entropy Alloys*, 2nd ed. Elsevier, **2011**.

[46] J. Das, G. Appa Rao, and S. K. Pabi, “Microstructure and mechanical properties of tungsten heavy alloys,” *Mater. Sci. Eng. A*, vol. 527, no. 29–30, pp. 7841–7847, **2010**.

[47] Z. Jiao, R. Kang, Z. Dong, and J. Guo, “Microstructure characterization of W-Ni-Fe heavy alloys with optimized metallographic preparation method,” *Int. J. Refract. Met. Hard Mater.*, vol. 80, no. 2018, pp. 114–122, **2019**.

[48] Z. A. Hamid, S. F. Moustafa, W. M. Daoush, F. A. Mouez, and M. Hassan, “Fabrication and Characterization of Tungsten Heavy Alloys Using Chemical Reduction and Mechanical Alloying Methods,” *Open J. Appl. Sci.*, vol. 03, no. 01, pp. 15–27, **2013**.

[49] . A. S. A., “Phases Identification By X- Ray Analysis for Liquid Phase Sintered

Tungsten Heavy Alloys," *Int. J. Res. Eng. Technol.*, vol. 06, no. 05, pp. 69–79, **2017**.

[50] A. Bose and R. M. German, "Sintering atmosphere effects on tensile properties of heavy alloys," *Metall. Trans. A*, vol. 19, no. 10, pp. 2467–2476, **Oct. 1988**.

[51] R. M. German, P. Suri, and S. J. Park, "Review: Liquid phase sintering," *J. Mater. Sci.*, vol. 44, no. 1, pp. 1–39, **2009**.

[52] R.M. German, *Liquid Phase Sintering - R.M. German - Google Books*. New York: Springer Science + Business Media, **1985**.

[53] G. . Schaffer, T. . Sercombe, and R. . Lumley, "Liquid phase sintering of aluminium alloys," *Mater. Chem. Phys.*, vol. 67, no. 1–3, pp. 85–91, **Jan. 2001**.

[54] K. Y. Tsai, M. H. Tsai, and J. W. Yeh, "Sluggish diffusion in Co-Cr-Fe-Mn-Ni high-entropy alloys," *Acta Mater.*, vol. 61, no. 13, pp. 4887–4897, **2013**.

[55] R. M. German, *Sintering With External Pressure*. **2014**.

[56] M. Hong, J. Noh, W. H. Baek, E. Kim, H. Song, and S. Lee, "A Study on the Improvement of the Sintered Density of W-Ni-Mn Heavy Alloy," vol. 28, no. October, pp. 835–839, **1997**.

[57] A. M. Ozbayoglu, N. Durlu, and N. K. Caliskan, "Automated Image Analysis and Contiguity Estimation for Liquid Phase Sintered Tungsten Heavy Alloys."

[58] "Glossary - at% and wt%." [Online]. Available: https://www.southampton.ac.uk/~pasr1/g7.htm. [Accessed: 29-Sep-2018].

[59] Carl R. (Rod) Nave, "Search Results," *Hyper Physics*, **2016**. [Online]. Available: http://hyperphysics.phy-astr.gsu.edu/hbase/thermo/adiab.html. [Accessed: 10-Nov-2017].